The Rydberg spectrum of CaF and BaF: Calculation by R-matrix and generalized quantum defect theory

M. Arif, Ch. Jungen, and A. L. Roche

Citation: The Journal of Chemical Physics **106**, 4102 (1997); doi: 10.1063/1.473124
View online: https://doi.org/10.1063/1.473124
View Table of Contents: http://aip.scitation.org/toc/jcp/106/10
Published by the American Institute of Physics

The Rydberg spectrum of CaF and BaF: Calculation by *R*-matrix and generalized quantum defect theory

M. Arif, Ch. Jungen, and A. L. Roche[a)]
Laboratoire Aimé Cotton du CNRS, Université de Paris-Sud, 91405 Orsay, France

(Received 29 October 1996; accepted 15 November 1996)

R-matrix theory combined with generalized quantum defect theory is used to calculate the electronic spectrum of the CaF and BaF molecules from the ground state up near the ionization limit. The approach, an effective one-electron method similar in spirit to the ligand-field model of Rice, Martin, and Field [S. F. Rice, H. Martin, and R. W. Field, J. Chem. Phys. **82**, 5023 (1985)] and to the electrostatic polarization model of Törring, Ernst, and Kändler [T. Törring, W. E. Ernst, J. Kändler, J. Chem. Phys. **90**, 4927 (1989)] removes many of the limitations inherent in the previous work. The resulting level energies (effective principal quantum numbers) are in good agreement with the available experimental data and constitute the first quantitative theoretical calculation of the full electronic spectrum of CaF and BaF. Limitations and possible extensions of the theory are discussed, and quantum defects of high orbital angular momentum states are predicted. © *1997 American Institute of Physics.* [S0021-9606(97)02607-X]

I. INTRODUCTION

The alkaline earth halides are prototypes of ionic molecules with a lone electron moving in the field of two closed-shell atomic ions, a metal ion M^{++} carrying two positive charges and a halogen ion X^- carrying a negative charge. This picture has been underlying most theoretical descriptions of these systems. In the early 1980's Rice, Martin, and Field[1] developed the so-called ligand-field model. They calculated the polarization of the lone electron orbital situated on the metal ion by the electrostatic field of the ligand ion which was treated as an external perturber. The calculation involves a state-by-state perturbation Hamiltonian matrix diagonalization and requires explicit knowledge of the M^+ valence electron wave functions. The model is capable of predicting the lowest Rydberg states of the alkaline earth halides, but its application to higher states is more difficult because of the rapid increase of the size of the basis sets required. A few years later Törring, Ernst, and Kändler[2] put forward an electrostatic polarization model. Here the energy is evaluated classically in terms of the mutual polarization of the two centers M^+ and X^- and the quadrupole moment of the valence electron wave function. Unlike the ligand-field model this approach is not based on the explicit knowledge of electron wave functions. While this model is very attractive in terms of the physical insight it provides, it has the drawback that the dipole polarizability of M^+ is treated as an adjustable parameter so that its predictive power is limited. This model has yielded excitation energies and dipole moments for the lowest excited states of several alkaline earth halides in quite good agreement with experiment. Only relatively few *ab initio* calculations have been made for alkaline earth halides, and these again do not extend beyond the first few excited electronic states.[3,4]

The experimental spectroscopic knowledge of the alkaline earth halides has vastly expanded since about 1990. Fourier-transform recorded laser induced emission spectra[5,6] yielded highly precise molecular constants for states ranging up to 4 eV above the ground state. Building on this information, Field and co-workers[7–9] carried out double resonance fluorescence experiments on several of these related molecules which opened up the region of the higher Rydberg states with effective principal quantum numbers ν ranging up to $\approx$15.

As Field and co-workers recognized, these Rydberg states no longer correspond to a metal ion ($M^{++}e^-$) perturbed by an external ligand X^-. They are more realistically described in terms of a Rydberg electron e^- moving in the field of an ionic closed-shell core ($M^{++}X^-$). Field and co-workers[7,8] summarized the present knowledge of CaF and BaF in compact form in a set of plots ν(mod1) vs ν, where ν is the effective principal quantum number (often called n^*) and ν(mod1) is the negative of the quantum defect. Numerous Rydberg series are apparent in these plots, whose quantum defects however are not constant in each series, but exhibit for low ν characteristic strong energy dependencies which are different for different series. These plots suggest that the ground states of CaF and BaF can each be associated with one of the series of $^2\Sigma^+$ symmetry of the corresponding molecule. Thus, *a priori* somewhat surprisingly, the alkaline earth monohalides can be regarded as ''Rydberg molecules,'' in the sense that all their states including the ground state naturally fit into Rydberg series. On the other hand it is not possible on experimental grounds alone to assign particular orbital angular momentum values l to the individual series. Indeed, the alkaline earth halides possess among the largest dipole moments known for diatomic molecules and hence one expects that there should be strong l mixing in their Rydberg states. For this reason Field and co-workers labeled each observed series by the high-ν value of ν(mod1) and its symmetry, e.g., $0.23^2\Sigma^+$. We shall use the same convention in this paper.

[a)]Laboratoire de Photophysique Moléculaire du CNRS, Université de Paris-Sud, 91405 Orsay, France.

 0021-9606/97/106(10)/4102/17/$10.00

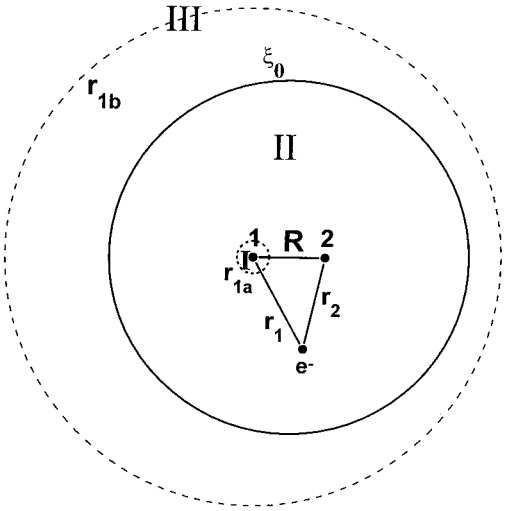

FIG. 1. Schematic representation of an electron interacting with an alkaline earth halide ion: 1, metal nucleus. 2, halogen nucleus. I, atomic zone. II, molecular (''reaction'') zone. III, asymptotic zone. The spheres $r=r_{1a}$, $r=r_{1b}$ and the ellipsoid $\xi=\xi_0$ are the boundaries used in the R-matrix calculation (cf. the text). The figure is drawn to the scale corresponding to the calculations carried out for CaF.

The vast amount of experimental data collected by the group of Field mainly on CaF and BaF constitutes a challenge to theorists, and the present work is a response to this. Our aim here is to provide a theory which describes both limiting situations, $(M^{++}e^-)X^-$ and $(M^{++}X^-)e^-$, equally well. While retaining the physical simplicity of the ligand field and electrostatic polarization models, the theory should yield reliable predictions of the full level spectrum up to the ionization potential and of the electron-ion phase shift spectrum in the ionization continuum beyond. A preliminary account of this work has been given previously.[9] In this work we calculate the bound energy level pattern for the equilibrium internuclear distance. A forthcoming paper[10] will report on dipole moments, the variation of quantum defects with internuclear distance as well as the evolution with energy of the continuum electron phase shifts.

Our method is based on scattering theory. It involves a variational one-electron R-matrix calculation in a limited volume surrounding the atomic cores M^{++} and X^- but which excludes the M^{++} core (cf. Fig. 1). We take advantage of the fact that on both boundaries of this reaction zone the electronic motion can be described quite simply:

(i) Inside the metal ion M^{++} intra-atomic forces prevail. Near the ion surface the electronic motion is therefore in a good approximation separable in a spherical coordinate system centered on M^{++} and it will be shown that the known quantum defects of $M^{++}e^-$ contain all the information needed to represent the wave function on the ion surface.

(ii) At large electron distances the field of the molecular $(M^{++}X^-)$ core reduces to that created by two point charges which are separated by the internuclear distance R. The electron motion therefore is separable in elliptic coordinates. It turns out that the long range field is not exactly that created by two elementary charges $+2$ and -1. Rather, mutual polarization of the atomic ions tends to partially compensate the electrostatic field so that the asymptotic field corresponds to that of two effective charges, reduced by as much as 20% to 40%.

The role of the R-matrix calculation is to propagate the electron wave function from the short-range atomic to the asymptotic region and thus to define the asymptotic molecular reactance matrix $K(\epsilon)$. The calculation is completed by an application of generalized quantum defect theory which determines bound or continuum states in terms of this reactance matrix.

Two related theoretical approaches may be mentioned here. The multiple scattering method (MSM) developed for molecules in the 1970's by Dill and Dehmer[11] also involves the calculation of reaction matrices by means of matching procedures applied simultaneously on the boundaries of the individual atoms and of the whole molecule. The main element of our approach, namely the variational evaluation of the electron motion in the intermediate zone with a realistic potential field, was however not present in the earlier work, nor was use made of the generalized form of quantum defect theory. Philippe, Masnou-Seeuws, and Valiron[12] and more recently Du and Greene[13] considered alkali atoms with neutral perturbers (rare gas atoms). Reference 12 focused on the realistic representation of the one-electron potential as we do here, but rather than using R-matrix theory, represented the perturber core by orthogonality constraints imposed on the wave function. The method of Ref. 13 is perturbative in that only s- and p-wave scattering on the perturber is taken into account, but otherwise is quite close to the present approach.

II. THEORY

Figure 1 illustrates the partitioning of space into different zones which we use. We discuss the electron wave function in the various regions in turn. Rydberg energy units are used throughout.

A. Atomic zone I

When the Rydberg electron enters either of the constituent ions it will experience many-electron interactions and there is no simple description of its motion. We assume here that the repulsive potential of the halogen ion X^- prevents significant electron penetration. Therefore it will be sufficient to describe the $X^- - e^-$ interaction by a local potential of appropriate form. (In fact, penetration effects can also be included within the present theory as long as they can be represented by a local one-electron potential.) On the other hand there will be strong penetration of the Rydberg electron wave function into the metal ion. We will therefore exclude the sphere $r_1 \leqslant r_{1a}$ surrounding the nucleus of M^{++} (cf. Fig. 1) from our calculations and replace the many-electron wave function inside the metal ion by a set of appropriate boundary conditions on the Rydberg electron wave function at $r_1 = r_{1a}$.

Specifically we write for each partial component l,

$$\psi_l^I(\epsilon_1,r_1,\theta_1,\phi)=Y_{l\lambda}(\theta_1,\phi)\,\frac{1}{r_1}\,[f_l(\epsilon_1,r_1)\cos\,\pi\mu_l - g_l(\epsilon_1,r_1)\sin\,\pi\mu_l], \tag{1}$$

where the $Y_{l\lambda}$ are ordinary spherical harmonics centered on the metal nucleus. λ here and later is the projection of the orbital angular momentum on the internuclear axis which remains a good quantum number in the diatomic system and within the present framework is identical with the spectroscopic quantum number Λ.

f_l and g_l are energy-normalized radial wave functions also centered on the metal nucleus which are regular and irregular, respectively, at the origin $r_1=0$. The μ_l are the quantum defects of the free metal ion M^+. ϵ_1 is an effective collision energy which will be specified in Sec. III A. If f_l and g_l are taken to be radial Coulomb functions, Eq. (1) will be valid for the free ion for values r_1 sufficiently large so that the polarization field is negligible. The quantum defects μ_l are then directly those obtained from the M^+ energy levels ϵ_{nl} by means of the Rydberg equation in Rydberg units, $\epsilon_{nl}=-1/[(n-\mu_l(\epsilon)]^2$. Here we shall instead define the radial functions f_l and g_l as the energy-normalized functions associated with the Coulomb potential including the polarization contribution (CP), namely,

$$V^{(\mathrm{CP})}(r_1)\approx-\frac{2Z_1}{r_1}-\frac{\alpha_1}{r_1^4}\,f_1^2(r_1) \tag{2}$$

[to which the centrifugal term $l(l+1)/r_1^2$ is to be added], where α_1 is the dipole polarizability of the metal core M^{++} and

$$f_1(r_1)=[1-e^{-(r_1/r_{1c})^6}]^{1/2} \tag{3}$$

is the customary cutoff function for the polarization potential with r_{1c} the ''core radius.'' With this definition Eq. (1) remains valid down to the metal core surface $r_1=r_{1a}\approx r_{1c}$. However the quantum defect μ_l now no longer corresponds to the value which would be obtained from the Rydberg equation. Instead, μ_l in Eq. (1) represents the core contribution to it, whereas the polarization contribution is effectively absorbed into the radial functions f_l and g_l. At the same time the radial functions no longer are the analytical Coulomb functions defined by Seaton,[14] but they must be calculated numerically. Our method of doing this will be described elsewhere;[15] it is an extension of the phase-amplitude formulation of generalized quantum defect theory given by Greene, Rau, and Fano.[16] In the following it will be assumed that intra-atomic forces still prevail in the molecular environment near $r_1\approx r_{1a}$ so that Eq. (1) remains valid. With f_1, g_l and μ_l known, Eq. (1) thus establishes a boundary condition at $r_1=r_{1a}$ which for each partial component l ensures the continuity of the wave function across the core boundary. This condition is

$$-\frac{\partial(r_1\psi_l^I)/\partial r_1}{(r_1\psi_l^I)}=-\frac{\partial(r_1\psi_l^{II})/\partial r_1}{(r_1\psi_l^{II})}=b_l(r_1), \tag{4}$$

where for the given core radius ($r_1=r_{1a}$) the set of quantities b_l depends smoothly on the energy and characterizes the particular metal ion $M^{++}e^-$. Each term of the partial wave expansion of Ψ^{II} valid in the reaction zone II of Fig. 1 must then satisfy Eq. (4).

B. Reaction zone II

We next construct a set of variational solutions Ψ_β^{II} which satisfy Eq. (4) and are valid throughout the reaction II surrounding the atomic zone I (see Fig. 1). We write the potential for $r_1\geqslant r_{1a}$ by taking account of the following:

(a) the Coulomb interaction between Z_1, Z_2, and e^-;
(b) the energy of the electric dipole induced on each ion by the electron and by the charge of the other ion;
(c) the dipole–dipole interaction energy of each electron-induced dipole on one center with the ion-induced dipole on the other center;
(d) the dipole–dipole interaction energy of the two electron-induced dipoles;
(e) a small metal core correction potential which will be specified in Sec. III B;
(f) all the terms that are independent of the position of the electron (such as e.g. the dipole–dipole interaction energy between the dipoles induced on each ion by the other ion) are part of the energy of the ion core and are therefore not considered explicitly.

We thus have

$$V_l(\mathbf{r}_1,\mathbf{r}_2,R)=-\left[\frac{2Z_1}{r_1}+\frac{2Z_2}{r_2}\right]+\left[-\alpha_1 f_1^2\,\frac{1}{r_1^4}+\alpha_1 f_1\,\frac{2Z_2\cos\,\theta_1}{r_1^2R^2}-\alpha_2 f_2^2\,\frac{1}{r_2^4}+\alpha_2 f_2\,\frac{2Z_1\cos\,\theta_2}{r_2^2R^2}\right]$$

$$-\frac{4\alpha_1 f_1\alpha_2 f_2}{R^5}\left[\frac{Z_1\cos\,\theta_1}{r_1^2}+\frac{Z_2\cos\,\theta_2}{r_2^2}\right]+\frac{2\alpha_1 f_1\alpha_2 f_2}{R^3 r_1^2 r_2^2}[2\cos\,\theta_1\cos\,\theta_2+\sin\,\theta_1\sin\,\theta_2]+V_l^{(\mathrm{core})}(r_1). \tag{5}$$

r_1 and r_2 are defined in Fig. 1. The polar angles θ_1 and θ_2 are defined such that $\theta_1=\theta_2=0$ at the molecular midpoint, α_1 and α_2 are the dipole polarizabilities of M^{++} and X^-, f_1 and f_2 are the cutoff functions for the polarization potentials of the two centers defined in Eq. (3). The choice of the cutoff radii r_{1c} and r_{2c} entering f_1 and f_2 will be specified in Sec. III D. The five terms of Eq. (5) correspond, in this order, to the terms (a)–(e) mentioned above.

We are now ready to set up a basis of functions which will be used in the variational determination of the solutions describing the electron motion for $r_1 \geqslant r_{1a}$. We chose a basis defined for $r_{1a} \leqslant r_1 \leqslant r_{1b}$ (see Fig. 1) where r_{1b} will be chosen as specified in Sec. III E. The basis consists of spherical free-particle eigenfunctions for positive and negative energy as follows:

$$\begin{aligned}\psi_{ml}^{(\lambda)}(r_1,\theta_1,\phi) &= Y_{l\lambda}(\theta_1,\phi)\,\frac{1}{r_1}\,[c_{ml}\,\sin(k_{ml}r_1) \\ &\quad + d_{ml}\,\cos(k_{ml}r_1)], \\ &\quad \left[\epsilon_{ml}^{(\lambda)}=\frac{1}{2}\,k_{ml}^2 \geqslant 0\right], \\ \psi_{ml}^{(\lambda)}(r_1,\theta_1,\phi) &= Y_{l\lambda}(\theta_1,\phi)\,\frac{1}{r_1}\,[c_{ml}e^{\kappa_{ml}r_1}+d_{ml}e^{-\kappa_{ml}r_1}], \\ &\quad \left[\epsilon_{ml}^{(\lambda)}=-\frac{1}{2}\,\kappa_{ml}^2 \leqslant 0\right].\end{aligned} \tag{6}$$

The coefficients c_{ml} and d_{ml} are determined by imposition of specific boundary conditions at $r_1=r_{1a}$ and $r_1=r_{1b}$. At the inner edge of zone II we impose the set of conditions Eq. (4), whereas the condition imposed at the outer edge is arbitrary but fixed and will be specified in Sec. III F. For a given set of conditions $b_l(r_{1a})$ and $b_l(r_{1b})$ this procedure yields a discrete set of energies $\epsilon_{ml}^{(\lambda)}$ and eigenfunctions which are orthonormalized. This is described in the Appendix A.

We next set up a Hamiltonian matrix for each value of λ with elements given by the volume integrals

$$\begin{aligned}H_{ml,m'l'}^{(\lambda)}(R) &= +\epsilon_{ml}^{(\lambda)}\delta_{ml,m'l'} + \int\int\int \psi_{ml}^{(\lambda)*}(r_1,\theta_1,\phi) \\ &\quad \times\left[V_l(\mathbf{r}_1,\mathbf{r}_2,R)+\frac{l(l+1)}{r_1^2}\right] \\ &\quad \times\psi_{m'l'}^{(\lambda)}(r_1,\theta_1,\phi)r_1^2\,\sin\,\theta_1 dr_1 d\theta_1 d\phi.\end{aligned} \tag{7}$$

The matrix is of course diagonal in λ.

Diagonalization of this matrix in principle yields eigenvalues and eigenfunctions of the one-electron Hamiltonian valid in the range $r_{1a} \leqslant r_1 \leqslant r_{1b}$ which at $r_1=r_{1a}$ reduce to a superposition of atomic functions $\psi_l^I(r_{1a})$ as required by Eq. (1). These eigenenergies and eigenfunctions also depend on the boundary condition $b(r_{1b})$ imposed at the outer boundary $r_1=r_{1b}$. $b(r_{1b})$ may be varied iteratively, and each time an eigenvalue of **H** coincides with the preselected energy ϵ, b is an eigenvalue of the boundary condition. This is the iterative eigenchannel R-matrix procedure of Fano and Lee.[17]

In the variational R-matrix scheme such as formulated by Greene[18] one solves a generalized eigenvalue system of the form

$$\mathbf{\Gamma a}=b(r_{1b})\mathbf{\Lambda a} \tag{8}$$

which directly yields the set of eigenvalues b_β ($\beta=1,2,...$) for the boundary condition on the outer sphere $r_1=r_{1b}$. The associated set of coefficients $a_{ml,\beta}$ serves to construct the eigenfunctions valid in the reaction zone II in terms of the basis of Eq. (6),

$$\Psi_\beta^{\mathrm{II}}=\sum_{m,l}\,a_{ml,\beta}^{(\lambda)}\psi_{ml}^{(\lambda)} \tag{9}$$

for each ϵ, R, and λ. For a given preselected total energy ϵ the matrices $\mathbf{\Gamma}$ and $\mathbf{\Lambda}$ are defined as follows:[18]

$$\begin{aligned}\Gamma_{ml,m'l'}^{(\lambda)}(\epsilon,R) &= -H_{ml,m'l'}^{(\lambda)}(R)+\epsilon\delta_{ml,m'l'} \\ &\quad -\int\int\,[r_{1b}\psi_{ml}^{(\lambda)}(r_{1b},\theta_1,\phi_1)] \\ &\quad \times\frac{\partial}{\partial r_1}\,[r_1\psi_{ml\lambda}(r_1,\theta_1,\phi_1)]_{r_1=r_{1b}} \\ &\quad \times\sin\,\theta_1 d\theta_1 d\phi_1, \\ \Lambda_{ml,m'l'}^{(\lambda)} &= +\int\int\,\psi_{ml}^{(\lambda)}(r_{1b},\theta_1,\phi_1) \\ &\quad \times\psi_{m'l'}^{(\lambda)}(r_{1b},\theta_1,\phi_1)r_{1b}^2\,\sin\,\theta_1 d\theta_1 d\phi_1,\end{aligned} \tag{10}$$

where the angular integrations yield $\delta_{ll'}\delta_{\lambda\lambda'}$ by virtue of Eq. (6) while the Hamiltonian matrix elements $H_{ml,m'l'}^{(\lambda)}$, those of Eq. (7), are nondiagonal in l.

C. Asymptotic zone III

The next step of the calculation consists in matching the eigensolutions $\Psi_\beta^{\mathrm{II}}(r_1,\theta_1,\phi_1)$ of the reaction zone to eigenfunctions of the separable asymptotic Hamiltonian and hence to determine the desired reaction matrix **K**. We first consider the asymptotic behavior of the potential $V(\mathbf{r}_1,\mathbf{r}_2)$ of Eq. (5). Expressing V in terms of elliptic coordinates

$$\begin{aligned}\xi &= \frac{r_1+r_2}{R}\;(1\leqslant\xi\leqslant\infty), \\ \eta &= \frac{r_1-r_2}{R}\;(-1\leqslant\eta\leqslant+1), \\ \phi &= \phi_1,\end{aligned} \tag{11}$$

we show easily that for large r_1 and r_2 such that $\xi \gg 1 \gg \eta$,

$$\begin{aligned}V(\mathbf{r}_1,\mathbf{r}_2,R) \approx -\frac{4}{R(\xi^2-\eta^2)}\Bigg\{\left[(Z_1+Z_2)+\frac{4}{R^3\xi^3}(\alpha_1+\alpha_2)\right]\xi \\ -(Z_1^{\mathrm{eff}}-Z_2^{\mathrm{eff}})\,\eta\Bigg\},\end{aligned} \tag{12}$$

with

$$Z_1^{\rm eff}=Z_1\left(1-\frac{2\alpha_2}{R^3}-\frac{4\alpha_1\alpha_2}{R^6}\right), \tag{13}$$

and where $Z_2^{\rm eff}$ is defined accordingly. Equation (12) is the potential of two electric point charges expressed in elliptic coordinates, with two differences.

(i) The total charge of the Coulomb term is complemented by a polarization term proportional to the sum of the dipole polarizabilities of the two ions which decreases with ξ^{-4};

(ii) the charge difference of the dipole term is replaced by the difference of two *effective* charges $Z_1^{\rm eff}$ and $Z_2^{\rm eff}$ as given by Eq. (13). This equation expresses the fact that mutual polarization of the two centers tends to compensate the dipole field created by the ion charges. Specifically the effective reduction of Z_1, proportional to the polarizability α_2, accounts for the fact that the center of the electron charge on the second atom is displaced by the polarization. Miecznik and Greene[19] have studied this effect in detail for the $He^{++}F^-$ system.

The electron motion in the potential $V(\xi,\eta)$ of Eq. (12) is well-known to be separable (see Appendix B). The relevant equations are collected for easy reference in the Appendix B. Solution of the Schrödinger equation yields dipolar angular functions $\tilde{Y}_{\tilde{l}\lambda}(\eta,\phi)$ which are just dipole distorted spherical harmonics. In the present context we require energy-normalized radial regular and irregular functions $\tilde{f}_{\tilde{l}}(\epsilon,\xi)$ and $\tilde{g}_{\tilde{l}}(\epsilon,\xi)$ which we evaluate numerically following Refs. 15 and 16. Examples of dipolar orbitals $\tilde{Y}_{\tilde{l}\lambda}(\eta,\phi)\tilde{f}_{\tilde{l}}(\xi)$ are illustrated in the Appendix B below.

D. Evaluation of the K matrix

We next choose a value ξ_0 in order to match each solution $\Psi_\beta^{(\lambda)}$ obtained in zone II to asymptotic functions valid in region III. With ξ_0 large enough so that Eq. (12) holds we can use the following expansion:

$$\Psi_\beta^{\rm II}(\epsilon,\xi_0,\eta,\phi)=\Psi_\beta^{\rm III}(\epsilon,\xi_0,\eta,\phi)$$
$$\equiv\sum_{\tilde{l}}\tilde{Y}_{\tilde{l}\lambda}(\epsilon,\eta,\phi)\frac{1}{\sqrt{\xi_0^2-1}}[\tilde{f}_{\tilde{l}}(\epsilon,\xi_0)I_{\tilde{l}\beta}(\epsilon)$$
$$-\tilde{g}_{\tilde{l}}(\epsilon,\xi_0)J_{\tilde{l}\beta}(\epsilon)]. \tag{14}$$

(For the sake of clarity the indices λ and R on Ψ, $\tilde{f}$, $\tilde{g}$, I, and J are omitted here and later.) Equation (14) is entirely analogous to Eq. (1) except that it includes a sum over partial (dipolar) waves $\tilde{l}$ since unlike l in the free ion M^+, $\tilde{l}$ is not preserved in general in the MX molecule. The desired reaction matrix **K** or the equivalent quantum defect matrix μ then become

$$K_{\tilde{l}\tilde{l}'}^{(\lambda)}(\epsilon,R)\equiv\tan\,\pi\mu_{\tilde{l}\tilde{l}'}^{(\lambda)}(\epsilon,R)=\sum_\beta J_{\tilde{l}\beta}(\epsilon)I_{\beta\tilde{l}'}^{-1}(\epsilon). \tag{15}$$

The tan function in Eq. (15) is taken for each element individually. **I** and **J** are determined by the requirement that Eq. (14) and its derivative with respect to ξ be continuous at $\xi=\xi_0$. First, $\Psi_\beta^{\rm II}$ and its derivative are expanded in terms of the ''surface harmonics'' $\tilde{Y}_{\tilde{l}\lambda}$ with expansion coefficients

$$u_{\tilde{l}\beta}(\xi_0)=\int\int\tilde{Y}_{\tilde{l}\lambda}^*(\eta,\phi)[\sqrt{\xi_0^2-1}\Psi_\beta^{\rm II}(\xi_0,\eta,\phi)]d\eta d\phi, \tag{16}$$

and an analogous equation for u' (where the prime refers to differentiation with respect to ξ). Then Eq. (16) and its derivative are subtracted from each other after multiplication by $\tilde{g}'_{\tilde{l}}$ and $\tilde{g}_{\tilde{l}}$ or $\tilde{f}'_{\tilde{l}}$ and $\tilde{f}_{\tilde{l}}$, respectively. Since the Wronskian of $\tilde{f}_{\tilde{l}}$ and $\tilde{g}_{\tilde{l}}$ is equal to $1/\pi$ (see Refs. 16 and 15) it follows that

$$I_{\tilde{l}\beta}=\pi(\tilde{g}'_{\tilde{l}}u_{\tilde{l}\beta}-\tilde{g}_{\tilde{l}}u'_{\tilde{l}\beta}),$$
$$J_{\tilde{l}\beta}=\pi(\tilde{f}'_{\tilde{l}}u_{\tilde{l}\beta}-\tilde{f}_{\tilde{l}}u'_{\tilde{l}\beta}). \tag{17}$$

Use of Eq. (15) completes the calculation of the reaction matrix **K**.

E. Bound states

Bound states are found by writing a general superposition of asymptotic channel functions expressed in terms of **K** which now embodies all short-range scattering effects in regions II and I. Thus,

$$\Psi(\epsilon)=\sum_{\tilde{l},\tilde{l}'}\tilde{Y}_{\tilde{l}\lambda}\frac{1}{\sqrt{\xi^2-1}}$$
$$\times[\tilde{f}_{\tilde{l}}(\epsilon,\xi)\delta_{\tilde{l}\tilde{l}'}-\tilde{g}_{\tilde{l}}(\epsilon,\xi)K_{\tilde{l}\tilde{l}'}]Z_{\tilde{l}'}(\epsilon). \tag{18}$$

We must choose the expansion coefficients $Z_{\tilde{l}}(\epsilon)$ such that $\Psi(\epsilon)\to 0$ for $\xi\to\infty$. The asymptotic behavior of $\tilde{f}_{\tilde{l}}$ and $\tilde{g}_{\tilde{l}}$ is written in the phase-amplitude approach[16,15] as

$$\tilde{f}_{\tilde{l}}(\xi)\approx\sqrt{\frac{1}{\pi}}\,\alpha_{\tilde{l}}(\epsilon,\xi)\sin\,\beta_{\tilde{l}}(\epsilon),$$
$$\tilde{g}_{\tilde{l}}(\xi)\approx-\sqrt{\frac{1}{\pi}}\alpha_{\tilde{l}}(\epsilon,\xi)\cos\,\beta_{\tilde{l}}(\epsilon), \tag{19}$$

where the amplitude factor $\alpha_{\tilde{l}}(\epsilon,\xi)$ is exponentially divergent for negative ϵ values (bound state region) and $\beta_{\tilde{l}}(\epsilon)$ is the accumulated phase (whose dependence on λ and R is again not indicated for the sake of clarity). $\beta_{\tilde{l}}(\epsilon)$ measures the (generally nonintegral) number of half-oscillations of the wave function at the energy ϵ and is calculated with the methods introduced in Refs. 16 and 15. Application of the bound state boundary condition then leads to the familiar homogeneous linear system of MQDT, namely,

$$\sum_{\tilde{l}'}[\tan\,\beta_{\tilde{l}}(\epsilon)\delta_{\tilde{l}\tilde{l}'}+K_{\tilde{l}\tilde{l}'}]Z_{\tilde{l}'}(\epsilon)=0 \tag{20a}$$

for each $\tilde{l}$. Nontrivial solutions of Eq. (20a) occur only when the corresponding determinant is zero. Such zeros occur only for discrete values of the energy, $\epsilon_n=-1/\nu_n^2$, for each value

of λ. The corresponding defects $\mu_n = -\nu_n(\mathrm{mod}1)$ will be referred below as ''effective quantum defects.'' The coefficients $Z_{\tilde{l}'}(\epsilon_n)$ give the channel mixing for each bound state. An alternative equivalent form of the homogeneous linear system is

$$\sum_{\tilde{l}'} [\sin \beta_{\tilde{l}}(\epsilon) C_{\tilde{l}\tilde{l}'} + \cos \beta_{\tilde{l}}(\epsilon) S_{\tilde{l}\tilde{l}'}] B_{\tilde{l}'}(\epsilon) = 0, \qquad (20b)$$

where $\mathbf{K} = \mathbf{S}\mathbf{C}^{-1}$, $B = \mathbf{C}^{-1}Z$ and $\mathbf{S} = \mathbf{U} \sin \pi\mu \mathbf{U}^{-1}$ (and similarly for $\mathbf{C}$), with $\mathbf{U}$ representing the eigenvector matrix of the reaction matrix $\mathbf{K}$ of Eq. (20a) and $\tan \pi\mu$ its eigenvalues.

III. DETAILS OF CALCULATION

A. Effective electron–metal atom collision energy

In order to connect each atomic radial function of Eq. (1) of region I to the set of molecular basis functions Eq. (6) of region II with the same l we must specify the effective electron–metal atom collision energy ϵ_1 occurring in Eq. (1) which corresponds to the classical kinetic electron energy in the vicinity of the metal nucleus. With Eq. (5), setting $r_2 \approx R \geqslant r_{2c}$, $\theta_2 \approx 0$ and taking the mean values of $\sin \theta_1$ and $\cos \theta_1$ near the metal nucleus to be zero, we find

$$\epsilon - V_l(\mathbf{r}_1, \mathbf{r}_2, R) \approx \left[\epsilon + \frac{2Z_2}{R} + \frac{\alpha_2}{R^4}\left(1 - 2Z_1 + 4\frac{\alpha_1 f_1 Z_2}{R^3}\right)\right] - \left[-\frac{2Z_1}{r_1} - \frac{\alpha_1}{r_1^4} f_1^2\right]. \qquad (21)$$

We recognize the last bracket $[\cdots]$ as being the atomic potential of Eq. (2). The first bracket therefore represents an effective collision energy,

$$\epsilon_1 = \epsilon + \frac{2Z_2}{R} + \frac{\alpha_2}{R^4}\left(1 - 2Z_1 + 4\frac{\alpha_1 f_1 Z_2}{R^3}\right). \qquad (22)$$

Equation (22) relates the molecular electron energy ϵ to the ''local'' atomic collision energy ϵ_1. The significance of this expression can be understood e.g. by considering a molecular threshold electron ($\epsilon = 0$). As the electron approaches from infinity, it is slowed down by the repulsive potential of the negative charge on the halogen atom [negative term $2Z_2/R$ in Eq. (22)] which would be absent in the isolated M^+ ion. As a result the effective energy near M^{++} is diminished. The additional terms in Eq. (22) are polarization corrections.

B. Logarithmic derivatives $-b_l(r_{1a})$

The logarithmic derivatives $-b_l(r_{1a})$ are the main dynamical parameters of the problem. In principle they can be evaluated from the known M^+ quantum defects as outlined in Sec. III A. In practice a difficulty arises since Eq. (22) shifts the effective collision energy by more than $\frac{1}{2}$Ry towards lower energies ($Z_2 = -1$, $R \approx 4$ a.u.). As a result the lower part of the MX Rydberg spectrum ($\nu \approx 2$) corresponds to an effective collision energy equivalent to $\nu \approx 1.5$ for which most of the empirical atomic quantum defects μ_l must be obtained through an extrapolation from higher energies.

TABLE I. Pseudopotential parameters for Ca and Ba.[a]

	$Ca^{++}e^-$				$Ba^{++}e^-$			
	$l=0$	1	2	⩾3	0	1	2	⩾3
$a_1^{(l)}$	4.0099	4.2056	3.5058	3.7741	3.0751	3.2304	3.2961	3.6237
$b_1^{(l)}$	13.023	12.658	12.399	13.232	2.6107	2.9561	3.0248	6.7416
$c_1^{(l)}$	2.1315	2.0186	−2.2648	3.1848	1.2026	1.1923	1.2943	2.0379
$r_{1c}^{(l)}$	1.6352	1.5177	1.6187	0.7150	2.6004	2.0497	1.8946	1.0473

[a]M. Aymar and M. Telmini, Ref. 20.

This extrapolation can be avoided if we represent the atomic core region by a suitable pseudopotential. Such potentials are available in the literature for several alkaline earth atomic ions M^+.[20] Their form is

$$V_l^{(\mathrm{core})}(r_1) = -\frac{2}{r_1}[(Z_{n1} - Z_1)e^{-a_1^{(l)} r_1} + b_1^{(l)} r_1 e^{-c_1^{(l)} r_1}] + \frac{\alpha_1}{r_1^4}\{e^{-[r_1/r_{1c}^{(l)}]^6} - e^{-(r_1/r_{1c})^6}\}. \qquad (23)$$

Z_{n1} is the charge of the metal nucleus while Z_1 is the metal ion charge as before. The first two terms in Eq. (23) represent the screening of the metal nucleus by the core electrons, whereas the last term makes the polarization potential cutoff l-dependent. The pseudocharacter of the potential $V_l^{(\mathrm{core})}$ comes in through the l-dependence of the parameters $a_1^{(l)}$, $b_1^{(l)}$, $c_1^{(l)}$, and $r_{1c}^{(l)}$. $V_l^{(\mathrm{core})}(r_1)$ is defined for all $r_1 \geqslant 0$ and is added to the long-range Coulomb plus polarization potential $V^{(\mathrm{CP})}(r_1)$ from Eq. (2). Outside the M^{++} core $\{r_1 \geqslant [a_1^{(l)}]^{-1}, [c_1^{(l)}]^{-1}, r_{1c}^{(l)}\}$ $V_l^{(\mathrm{core})}$ becomes vanishingly small as stated before Eq. (5). With an appropriate choice of parameters[20] the combined effective potential $V^{(\mathrm{CP})}(r_1) + V_l^{(\mathrm{core})}(r_1) + l(l+1)/r_l^2$ can be made to represent the observed M^+ energy levels quite accurately for each l value. Each $b_l(r_{1a})$ can thus be obtained without difficulty by outward numerical integration of the radial Schrödinger equation in this potential from $r_1 = 0$ to $r_1 = r_{1a}$. Table I lists the pseudopotential parameters for CaF^+ and BaF^+ from Ref. 20.

C. Ion polarizabilities

The metal ion dipole polarizabilities α_1 for Ca^{++} and Ba^{++} and α_2 for F^- are listed in Table II. The polarizability of the isolated F^- is known from *ab initio* theory[23] to be very large ($\approx 16\ a_0^3$). Based on measurements of MF ground state

TABLE II. Dipole polarizabilities, cutoff radii, and ion internuclear distances (atomic units).

	α_1[a]	r_{1c}	α_2[b]	r_{2c}	R[c]
$Ca^{++}F^-$	3.5	1.6	4.7	2.3	3.54
$Ba^{++}F^-$	11.4	2.6	4.7	2.3	3.93

[a]M. Aymar and M. Telmini, Ref. 20.
[b]T. Törring, W. E. Ernst, and S. Kindt, Ref. 21.
[c]Z. J. Jakubek, N. A. Harris, R. W. Field, J. A. Gardner, and E. Murad, Ref. 22.

dipole moments Törring, Ernst, and Kindt[21] recommend a much smaller ''saturated'' value ($\approx 4.7\ a_0^3$) which we use here. The correctness of this value is corroborated by consideration of the dipole moment Q_1 of the $M^{++}X^-$ ion core. According to Eq. (12) the dipole moment with respect to the midpoint between the nuclei is

$$Q_1 = \frac{R}{2}\,(Z_2^{\rm eff} - Z_1^{\rm eff}). \tag{24}$$

The effective point charges $Z_1^{\rm eff}$ and $Z_2^{\rm eff}$ in turn depend on the dipole polarizabilities α_1 and α_2 [Eq. (13)], and thus a relationship is established between the core dipole moment and the ion polarizabilities. Jakubek,[24] in an *ab initio* calculation on CaF^+, found $Q_1 = -4.4$ a.u. with respect to the molecular midpoint for $R = 3.538$ a.u. Inverting Eq. (24) and using Eq. (13) with the value for α_1 given in Table II we derive $\alpha_2 = 4.0\ a_0^3$ which agrees to within 15% with the value $\alpha_2 = 4.7\ a_0^3$ recommended by Törring *et al.*[21] We used the latter value for both the CaF and the BaF calculations.

D. Polarizability cutoff radii r_{1c} and r_{2c}

The polarization cutoff radius corresponds to the distance at which the long-range potential expansion begins to break down and thus is a measure of the core radius. We take r_{1c} for each metal core M^{++} to be equal to the largest of the $r_{1c}^{(l)}$ values of the pseudopotential given in Table I. r_{2c} is taken such that

$$\overline{r_{1c}} + r_{2c} = R, \tag{25}$$

where $\overline{r_{1c}}$ is the mean of the $r_{lc}^{(l)}$ $(l = 0-4)$ values from Table I. This choice is consistent with the picture of two ionic spheres that touch each other. We have verified that the results of the calculations do not depend critically on the values chosen for the cutoff radii. The parameters defining the potential of Eq. (5) are listed in Table II.

E. R matrix radii r_{1a}, r_{1b}, and ξ_0

The choice of r_{1a} is made according to the following criteria: Ideally, both $V^{(\rm CP)}(r_1)$ of Eq. (2) and $V_l(\mathbf{r}_1,\mathbf{r}_2,R)$ of Eq. (5) should be valid representations of the potential felt by the valence electron near $r_1 = r_{1a}$, i.e., their difference should be small. In practice it suffices that their difference be about constant across the sphere $r_1 \leqslant r_{1a}$ such that it is taken in account in the effective collision energy ϵ_1 [Eq. (22)]. For this reason we take r_{1a} smaller than the core radius r_{1c}. We can do this since with the $V_l^{(\rm core)}$ [Eq. (23)] the electron motion is correctly represented for $r_{1a} \leqslant r_1 \leqslant r_{1c}$. On the other hand, $|V_l(\mathbf{r}_1,\mathbf{r}_2,R)|$ itself should not be too large in this range in order to avoid unduly large Hamiltonian matrix elements in Eq. (7). With these considerations in mind we took values for r_{1a} close to the smallest of the cutoff radii $r_{1c}^{(l)}$ of Table I, namely, $r_{1a} = 0.8$ a.u. for Ca^{++} and $r_{1a} = 1.0$ a.u. for Ba^{++}. Again we verified that the results do not depend critically on the choice made.

The elliptical radius ξ_0 must be taken large enough so that Eq. (12) is a good approximation and at the same time the M^{++} core must be enclosed in the ellipsoid $\xi = \xi_0$. The latter in turn must be contained within the sphere $r_1 = r_{1b}$. These requirements lead to the conditions

$$\xi_0 \geqslant 1 + \frac{2r_{1a}}{R}, \quad r_{1b} \geqslant \frac{R}{2}\,(1+\xi_0). \tag{26}$$

In general it is preferable to reduce ξ_0 as much as possible in order to avoid strong ϵ dependences of $\mathbf{K}$ or μ. We found that $\xi_0 = 5$ is a good choice with Eqs. (12) and (5) differing by less than 1% everywhere except near $\eta = +1$ (halogen ion) where generally little probability amplitude is present. On the other hand for $\xi_0 \leqslant 3$ Eq. (12) begins to break down seriously both for $\eta \approx -1$ and $+1$. We carried out two sets of calculations with $\xi_0 = 5.0$ and 3.0, and $r_{1b} = 12.2$ and 7.9 a.u., respectively, and we found that the resulting solutions ν_n differ by less than 0.015 for all of the electronic states calculated, although some of the $\mu_{\tilde{l},\tilde{l}'}$ elements differ by more than this amount. $\mathbf{K}(\epsilon)$ was evaluated on a coarse energy mesh and the solutions ν_n determined by suitable interpolation.

F. R matrix basis set and boundary conditions for $r_1 = r_{1b}$

We have included values $l = \tilde{l} = \lambda$ to 5 both for CaF and BaF in the R-matrix basis Eq. (6) and in the asymptotic expansion Eq. (14). Following the recommendation of Greene and Aymar[25] we took for each l typically 13 ''closed'' radial functions $[b(r_{1b}) = 10^9]$ and 2 ''open'' radial basis functions $[b(r_{1b}) = 0]$. This choice permitted the use of the ''streamlined'' version of the variational eigenchannel R-matrix formulation.[25] Convergence was checked in all cases. We found that for all $\tilde{l}', \tilde{l}$ with $\tilde{l} \geqslant 4$ and $\tilde{l}'$ arbitrary the calculations yield off-diagonal elements $|\mu_{\tilde{l}',\tilde{l}}| \leqslant 0.02$ and diagonal elements $|\mu_{\tilde{l},\tilde{l}}| \leqslant 0.002$. Accordingly the positions of the $\tilde{l} \geqslant 4$ states will be calculated below as corresponding to strictly nonpenetrating orbitals with all quantum defects $\mu_{\tilde{l},\tilde{l}'}$ set to zero.

IV. RESULTS AND DISCUSSION

A. Accumulated phase parameter and quantum defect matrices

According to Eqs. (20) and (15) the energies ϵ_n of the bound state spectrum are determined by (i) the phase $\beta_{\tilde{l}}$ accumulated by the electron $\tilde{l}$ in the asymptotic field and (ii) the short-range quantum defect matrix $\mu_{\tilde{l},\tilde{l}'}$. The behavior of the phase parameters $\beta_{\tilde{l}}(\epsilon)/\pi$ is illustrated in Fig. 2 for CaF for $\lambda = 0$ and $\tilde{l} = 0-4$ and compared with the Coulomb values $\beta/\pi = \nu - l$ used in the ordinary quantum defect theory. When all quantum defects are zero [$\mathbf{K} = 0$ in Eq. (20a)], bound states occur in Fig. 2 whenever $\beta(\nu)/\pi$ is an integer. In a pure Coulomb field (dotted lines in Fig. 2) this happens for integral ν values. Notice how in CaF (full lines) the dipole field pushes the lowest level $(\beta/\pi = 1)$ to higher energy for $\tilde{l} = 2$, 3, and 4 (cf. also the discussion of high-$\tilde{l}$ states in Sec. IV C), whereas for $\tilde{l} = 0$ and 1 the strong attraction of the doubly charged metal ion causes the first level

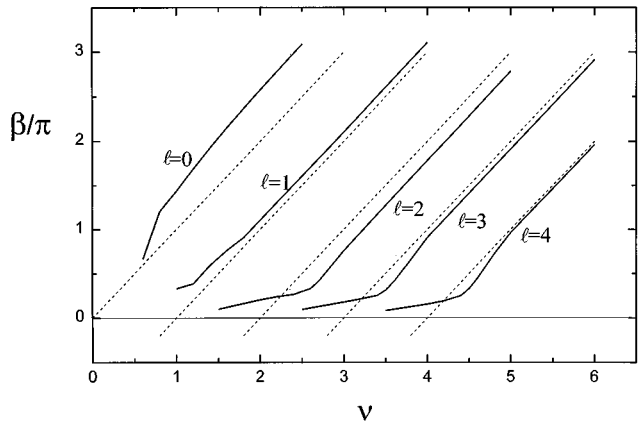

FIG. 2. Accumulated phase parameter β, in units of π, plotted as a function of the effective principal quantum number $\nu=(-\epsilon)^{-1/2}$ for $\tilde{l}=0-4$ and $\lambda=0$. Full lines, numerical values calculated with the potential Eq. (12) with parameters for CaF from Table II and $Z_1=2$, $Z_2=-1$. The dotted lines correspond to the phase parameter $\beta/\pi=\nu-l$ for a Coulomb field, used in ordinary quantum defect theory.

to occur *lower* than the hydrogenic state. This behavior is of course modified once the penetration effects embodied in the quantum defect matrix are taken into account.

Figure 2 illustrates further how the Coulomb accumulated phase parameter $\beta/\pi=\nu-l$ crosses the zero line for each l at $\nu=l$. This leads to unphysical solutions for $\nu\leqslant l$, a well-known difficulty in ordinary quantum defect theory.[14] This problem does not arise in the numerical approach used here,[15] since $\beta_{\tilde{l}}$ is seen to approach zero asymptotically as ν decreases below $\nu=\tilde{l}$. This physically correct feature is crucial for the success of the present calculations where we need to avoid false solutions in the $\nu\approx 1.5$ to 3 region while at the same time we must retain channels with relatively high $\tilde{l}$ values in the calculations.

Figure 3 illustrates the energy dependence of the elements $\mu_{\tilde{l},\tilde{l}'}$ with $\lambda=0$ for CaF. Two types of energy dependence can be discerned; all elements involving $\tilde{l}\geqslant 2$ approach zero for $\nu\leqslant 2.5$. This behavior originates from the corresponding behavior of the phase parameter $\beta_{\tilde{l}}$ depicted in Fig. 2. By contrast the substantial variations apparent in the figure for $\tilde{l}=0$ and 1 reflect more a resonant behavior. They are related to the fact that the lowest states with $\nu\leqslant 2.5$ are largely (and unavoidably) contained within the outer R-matrix radius r_{1b}. While this behavior is not incorrect as such, it renders the energy interpolations more difficult and probably is the origin of the somewhat less satisfactory agreement obtained in Sec. IV B for low ν than for high ν states.

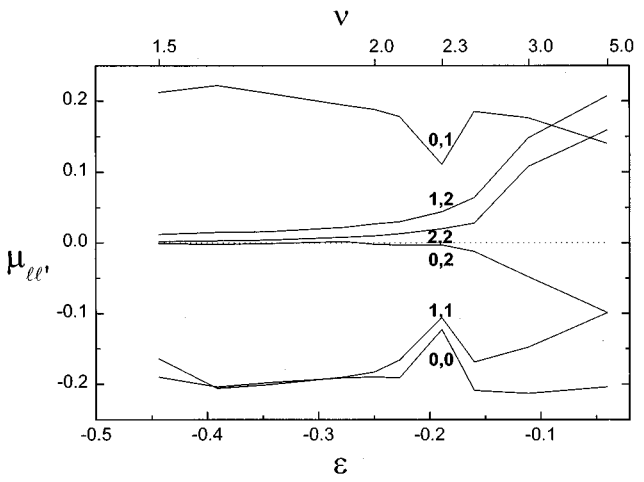

FIG. 3. Energy dependence of the quantum defect matrix elements $\mu_{\tilde{l},\tilde{l}'}$ for CaF with $\lambda=0$.

B. Energy levels

Tables III and IV summarize the effective principal quantum numbers ν_n obtained for the various values of λ for CaF and BaF, and compare them with the corresponding experimental values. The same data are represented graphically in the ν(mod1) vs ν plots of Fig. 4 (CaF) and Fig. 5 (BaF). The effective principal quantum number ν (abscissa) gives the overall position of the states on a nonlinear energy scale. The quantity ν(mod1) (ordinate), the effective principal quantum number stripped of its integral part in front of the decimal point, corresponds to the negative of the effective quantum defect and, per unit interval of ν, gives the relative positions of the states on an enlarged nonlinear energy scale. Tables III and IV and the plots show that on the whole the agreement between experiment and theory is quite gratifying. The mean deviation $|\nu_{\rm obs}-\nu_{\rm calc}|$ is 0.030 for CaF and 0.023 for BaF. This is equivalent to an error of the order of 650 $\rm cm^{-1}$ for $\nu\approx 2$ but of only ≈ 5 $\rm cm^{-1}$ for $\nu\approx 10$. This agreement is about a factor of 3 better than in our previous calculation[9] of the states of CaF which neglected polarization effects.

The main components $\tilde{l}'$ occurring in the expansion Eq. (20b) for $\nu\approx 5$ are listed for each series in Tables III and IV. As expected most of the series are strongly $\tilde{l}$ mixed. Note that this mixing occurs in addition to the mixing due to the asymptotic multipole field which causes each elliptic component l to be itself a mixture of spherical partial waves l. Thus it is clear that at least for low l it is not possible to assign even approximate l values to the individual series. The procedure of Jakubek and Field[8] who named each series by its asymptotic ν(mod1) value reached near $\nu\approx 5$, together with its molecular symmetry, thus remains valid.

Figures 4 and 5 show further that the characteristic observed positive or negative curvatures of the ν(mod1) curves at low ν are reproduced by the calculations for all of the series (the 0.14Δ series in CaF excepted), and that each series ends with the correct terminus state. All low lying states, including the $X\ ^2\Sigma^+$ ground state, are seen to fit naturally into the scheme of series. The empirical conclusion of Murphy *et al.*,[7] that the alkaline earth halides may be regarded as a particular type of ''Rydberg'' molecules, is thus supported by the theory. The success of the calculations shows indeed that the molecular core can be realistically represented by two separate scattering centers M^{++} and X^- if proper account is taken of polarization effects.

TABLE III. (a) $^2\Sigma^+$ Rydberg series of CaF. (b) $^2\Pi$ Rydberg series of CaF. (c) $^2\Delta$ Rydberg series of CaF. (d) $^2\Phi$ Rydberg series of CaF. The ionization potential of CaF is 46 998±5 cm^{-1}.[g] Each series is designated by $\nu_{\rm obs}$(mod1) taken for $\nu\approx 5$. For states with $\nu\leqslant 2.5$ a correction was applied which takes account of the difference of the vibrational frequency and internuclear distance in the molecular state and in the ion. The $\nu_{\rm obs}$ in the table thus correspond to vertical ionization energies corresponding to R_c of the ion. The spectral composition of each series is given for $\nu\approx 5$ in terms of the largest coefficients $B_{\tilde{l}}$, Eq. (20b).

(a)

$0.55\,^2\Sigma^+$ $0.99\tilde{s}+0.13\tilde{d}$			$0.88\,^2\Sigma^+$ $0.84\tilde{p}+0.51\tilde{d}+0.16\tilde{f}$			$0.18\,^2\Sigma^+$ $0.84\tilde{d}-0.53\tilde{p}-0.11\tilde{s}$			$0.09\,^2\Sigma^+$ $0.99\tilde{f}-0.13\tilde{p}-0.10\tilde{d}$		
$\nu_{\rm obs}$	$\nu_{\rm calc}$	$o-c$	$\nu_{\rm obs}$	$\nu_{\rm calc}$	$o-c$	$\nu_{\rm obs}$	$\nu_{\rm calc}$	$o-c$	$\nu_{\rm obs}$	$\nu_{\rm calc}$	$o-c$
X 1.536[a]	1.56	−0.02	*B* 1.991[b]	2.04	−0.05	*F′* 3.177[c]	3.17	+0.01		4.08	
D 2.553[d]	2.56	−0.01	*E* 2.925[e]	2.96	−0.03	4.183[a]	4.17	+0.01		5.08	
3.553[c]	3.55	+0.00	3.901[c]	3.90	+0.00	5.184[a]	5.16	+0.02		6.08	
	4.55		4.899[a]	4.86	+0.04	6.187[a]	6.16	+0.03		7.08	
5.551[a]	5.55	+0.00	5.880[a]	5.86	+0.02	7.189[a]	7.16	+0.03		8.08	
6.549[a]	6.55	−0.00	6.878[a]	6.86	+0.02	8.188[a]	8.16	+0.03		9.08	
7.546[a]	7.55	−0.00	7.871[a]	7.86	+0.01	9.196[a]	9.16	+0.04	10.087[f]	10.08	+0.01
8.549[a]	8.55	−0.00	8.868[a]	8.86	+0.01	10.173[f]	10.16	+0.01			
9.552[f]	9.55	+0.00	9.891[f]	9.86	+0.03						

(b)

	$0.98\,^2\Pi$ $1.00\tilde{p}$			$0.36\,^2\Pi$ $0.98\tilde{d}+0.18\tilde{f}$			$0.07\,^2\Pi$ $0.98\tilde{f}-0.18\tilde{d}$		
	$\nu_{\rm obs}$	$\nu_{\rm calc}$	$o-c$	$\nu_{\rm obs}$	$\nu_{\rm calc}$	$o-c$	$\nu_{\rm obs}$	$\nu_{\rm calc}$	$o-c$
	A 1.909[e]	1.92	−0.01	*C* 2.557[d]	2.55	+0.01		4.05	
	E′ 2.959[e]	2.97	−0.01	*F* 3.418[c]	3.45	−0.03		5.04	
	3.98[a]	3.97	+0.01	4.37[a]	4.41	−0.04		6.04	
	4.973[a]	4.97	+0.00	5.360[a]	5.40	−0.04		7.04	
	5.975[a]	5.97	+0.01	6.353[a]	6.40	−0.05		8.04	
	6.976[a]	6.97	+0.01	7.31[a]	7.40	−0.09		9.04	
	7.977[a]	7.97	+0.01	8.342[a]	8.40	−0.06	10.073[f]	10.04	+0.03
	8.976[a]	8.97	+0.01	9.348[a]	9.40	−0.05			
	9.98[a]	9.97	+0.01	10.384[f]	10.40	−0.02			
	11.007[f]	10.97	+0.04						

(c)

			$0.14\,^2\Delta$ $0.97\tilde{d}+0.23\tilde{f}$			$0.00\,^2\Delta$ $0.97\tilde{f}-0.23\tilde{d}$		
			$\nu_{\rm obs}$	$\nu_{\rm calc}$	$o-c$	$\nu_{\rm obs}$	$\nu_{\rm calc}$	$o-c$
			B′ 2.085[h]	2.16	−0.08		3.98	
				3.15			4.97	
			4.13[a]	4.15	−0.02		5.97	
			5.136[a]	5.15	−0.01		6.97	
			6.135[a]	6.15	−0.01		7.97	
			7.137[a]	7.15	−0.01		8.97	
			8.134[a]	8.15	−0.02	9.997[f]	9.97	+0.03
			9.131[a]	9.15	−0.02			
			10.170[f]	10.15	+0.02			

(d)

							$0.93\,^2\Phi$ $1.00\tilde{f}$	
							$\nu_{\rm calc}$	$o-c$
							3.89	
							4.89	
							5.89	
							6.88	
							7.88	
							8.88	
						9.934[f]	9.88	+0.05

[a]J. M. Berg, J. E. Murphy, N. A. Harris, and R. W. Field, Ref. 26.
[b]M. Dulick, P. F. Bernath, and R. W. Field, Ref. 27.
[c]N. A. Harris and R. W. Field, Ref. 28.
[d]C. M. Gittins, N. A. Harris, R. W. Field, J. Vergès, C. Effantin, A. Bernard, J. d'Incan, W. E. Ernst, P. Bündgen, and B. Engels, Ref. 29.
[e]P. F. Bernath and R. W. Field, Ref. 30.
[f]R. W. Field, N. A. Harris, and Ch. Jungen, Ref. 31.
[g]Z. J. Jakubek, N. A. Harris, R. W. Field, J. A. Gardner, and E. Murad, Ref. 22.
[h]J. Vergès, C. Effantin, A. Bernard, A. Topouzkhanian, A. R. Allouche, J. D'Incan, and R. F. Barrow, Ref. 5.

TABLE IV. (a) $^2\Sigma^+$ Rydberg series of BaF. (b) $^2\Pi$ Rydberg series of BaF. (c) $^2\Delta$ Rydberg series of BaF. (d) $^2\Phi$ Rydberg series of BaF. The ionization potential of BaF is $38\,742\pm3$ cm^{-1}.[a] Each series is designated by $\nu_{\rm obs}$(mod1) taken for $\nu\approx5$. For states with $\nu\leqslant2.5$ a correction was applied which takes account of the difference of the vibrational frequency and internuclear distance in the molecular state and in the ion. The $\nu_{\rm obs}$ in the table thus correspond to vertical ionization energies corresponding to R_e of the ion. The spectral composition of each series is given for $\nu\approx5$ in terms of the largest coefficients $B_{\tilde{l}}$, Eq. (20b).

(a)

$0.76\,^2\Sigma^+$ $0.92\tilde{s}+0.39\tilde{d}$			$0.88\,^2\Sigma^+$ $0.89\tilde{p}+0.37\tilde{d}-0.22\tilde{s}+0.14\tilde{f}$			$0.24\,^2\Sigma^+$ $0.82\tilde{d}-0.45\tilde{p}-0.32\tilde{s}+0.17\tilde{f}$			$0.08\,^2\Sigma^+$ $0.98\tilde{f}-0.21\tilde{d}$		
$\nu_{\rm obs}$	$\nu_{\rm calc}$	$o-c$	$\nu_{\rm obs}$	$\nu_{\rm calc}$	$o-c$	$\nu_{\rm obs}$	$\nu_{\rm calc}$	$o-c$	$\nu_{\rm obs}$	$\nu_{\rm calc}$	$o-c$
X 1.692[a]	1.72	−0.03	B 2.139[b]	2.14	−0.00	E 3.223[c]	3.23	−0.01	4.085[e]	4.08	+0.01
D 2.75[c]	2.75	−0.00	D' 2.963[c]	2.94	+0.02		4.24		5.078[f]	5.08	−0.00
G 3.758[e]	3.76	−0.00	H 3.922[e]	3.88	+0.04	5.242[f]	5.25	−0.01	6.081[f]	6.08	+0.00
4.760[f]	4.77	−0.01	4.895[f]	4.85	+0.05	6.240[f]	6.25	−0.01	7.087[f]	7.08	+0.01
5.766[f]	5.76	+0.01	5.887[f]	5.85	+0.04	7.248[f]	7.25	−0.00		8.08	
6.770[f]	6.76	+0.01	6.881[f]	6.85	+0.03	8.251[f]	8.25	−0.00		9.08	
	7.76		7.884[f]	7.85	+0.03	9.251[f]	9.25	+0.00	10.099[f]	10.08	+0.02
8.775[f]	8.76	+0.02	8.883[f]	8.85	+0.03				11.105[f]	11.08	+0.03
			9.889[f]	9.85	+0.04						

(b)

			$0.13\,^2\Pi$ $0.84\tilde{d}+0.50\tilde{p}+0.21\tilde{f}$			$0.45\,^2\Pi$ $0.87\tilde{p}-0.48\tilde{d}-0.13\tilde{f}$			$0.04\,^2\Pi$ $0.97\tilde{f}-0.25\tilde{d}$		
			A 2.047[b]	2.06	−0.01	C 2.459[c]	2.45	+0.01	K 4.033[e]	4.04	−0.01
			E' 3.109[g]	3.13	−0.02	F 3.440[c]	3.46	−0.02		5.03	
			J 4.127[e]	4.13	−0.00		4.47			6.03	
				5.14		5.447[f]	5.48	−0.03		7.03	
				6.14		6.449[f]	6.48	−0.03		8.03	
				7.14			7.48			9.03	
				8.14			8.48				

(c)

				$0.23\,^2\Delta$ $0.98\tilde{d}+0.19\tilde{f}$			$0.94\,^2\Delta$ $0.98\tilde{f}-0.20\tilde{d}$	
			A' 2.012[b]	2.02	−0.01	3.953[e]	3.96	−0.01
			E'' 3.102[e,g]	3.19	−0.09	4.945[f]	4.96	−0.01
				4.22		5.943[f]	5.95	−0.01
			5.227[f]	5.23	−0.00	6.945[f]	6.95	−0.00
			6.235[f]	6.23	+0.01		7.95	
			7.243[f]	7.23	+0.01	8.949[f]	8.95	−0.00
			8.246[f]	8.23	+0.02	9.955[f]	9.95	+0.01
			9.255[f]	9.23	+0.03			
			10.253[f]	10.23	+0.02			

(d)

$0.87\,^2\Phi$ $1.00\tilde{f}$		
	3.86	
	4.86	
	5.86	
	6.86	
	7.86	
	8.86	
9.867[f]	9.86	+0.01
10.873[f]	10.86	+0.01

[a]Z. J. Jakubek, N. A. Harris, R. W. Field, J. A. Gardner, and E. Murad, Ref. 22.
[b]A. Bernard, C. Effantin, J. D'Incan, J. Vergès, and R. F. Barrow, Ref. 35.
[c]C. Effantin, A. Bernard, J. D'Incan, G. Wannous, J. Vergès, and R. F. Barrow, Ref. 32.
[d]A. Bernard, C. Effantin, E. Andrianavalona, J. Vergès, and R. F. Barrow, Ref. 6.
[e]Z. J. Jakubek and R. W. Field, Ref. 33.
[f]Z. J. Jakubek, Ref. 34.
[g]C. Effantin, A. Bernard, J. D'Incan, E. Adrianavalona, and R. F. Barrow, Ref. 36.

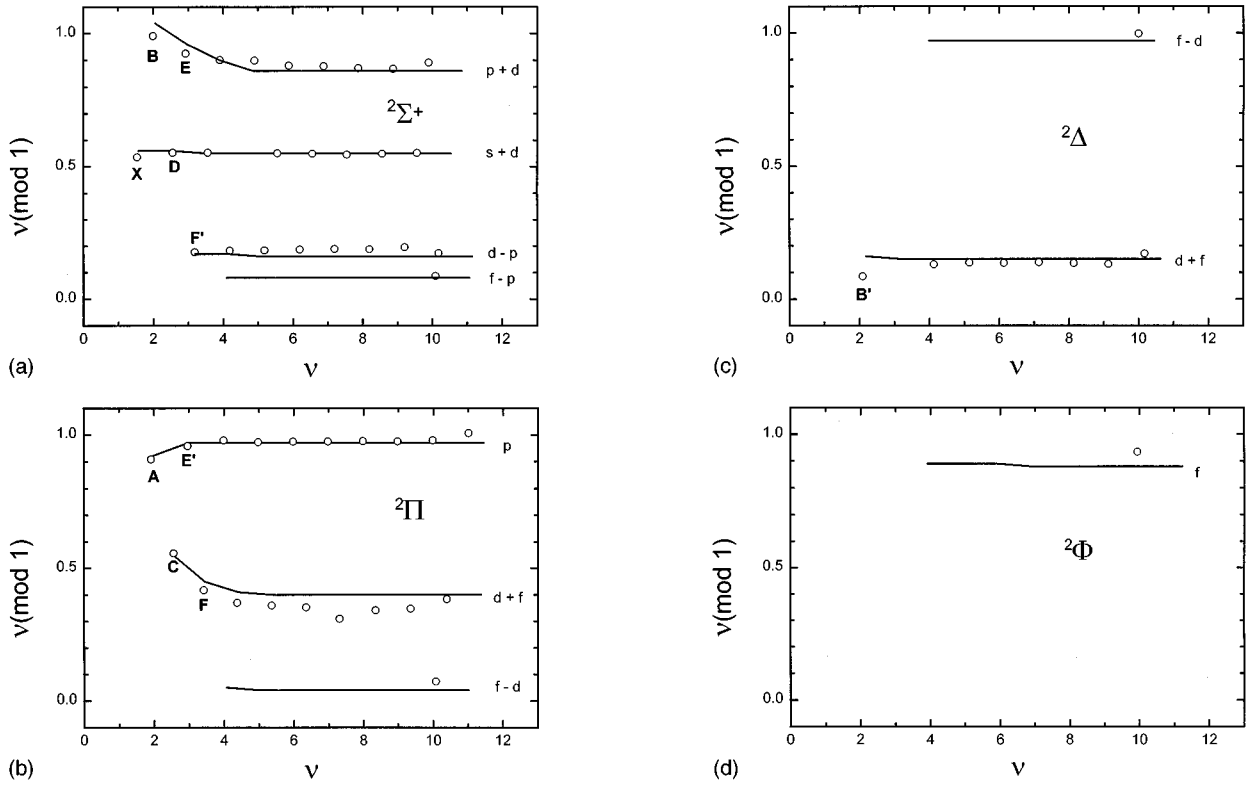

FIG. 4. Rydberg series of CaF. ν(mod1) of bound states is plotted vs ν, where ν is the effective principal quantum number and $\nu(\text{mod}1)=-\mu$ with μ the effective quantum defect. The abscissa thus represents the electron binding energy on the gross nonlinear scale $\nu=(-\epsilon)^{-1/2}$. For each unit interval the same information is represented on an enlarged scale on the ordinate. The spectral composition of each series for high ν in terms of elliptic components $\tilde{l}$ is indicated on the right. Circles, observed values. Full lines, calculated values. (a) $^2\Sigma$ states. (b) $^2\Pi$ states. (c) $^2\Delta$ states. (d) $^2\Phi$ states.

The comparison of the plots of Figs. 4 and 5 for CaF and BaF for corresponding symmetry Λ reveals that the patterns are basically similar in the two molecules. {For the Π symmetry this becomes apparent if one realizes that the 0.98Π series of CaF could be moved to the equivalent position -0.02 [Fig. 4(b)].} To make this analogy more complete we have reassigned the $B\ ^2\Sigma^+$ state of BaF as the terminus state of the $0.88^2\Sigma^+$ series instead of the $0.24^2\Sigma^+$ as proposed in Refs. 8 and 33. This reassignment is further justified since our calculations indicate that the B state has a predominantly $\tilde{p}$ character.

The calculations for BaF near $\nu\approx3.1$ yield one $^2\Pi$ and one $^2\Delta$ state whereas Effantin *et al.*[36] have assigned experimentally two $^2\Pi$ states in this region, E' and E'', separated by only 62 cm^{-1}, but no $^2\Delta$ state. The discrepancy can be resolved if, as is done in Table IV and Fig. 5(c) and was suggested very recently by Jakubek and Field,[33] E'' is assumed to be the missing $^2\Delta$ state. We note though, that the agreement obtained with this reassignment is less good than for the other states. Our calculations show further that near $\nu\approx4$ a few gaps still remain in the observations both for CaF and BaF. This intermediate region is difficult to reach by Fourier transform spectroscopy as well as by double resonance spectroscopy. For BaF we predict a series $0.13^2\Pi$ which has not yet been observed beyond $\nu\approx4$ [Fig. 5(b)].

C. Comparison with previous calculations of the lowest states

For some of the lower states of CaF and BaF there exist earlier theoretical calculations based on the polarization model, the ligand field approach or of *ab initio* type. These are collected in the Tables V and VI and compared with experiment and with our results. Also given are the deviations observed minus calculated and their rms value for the set of states for each calculation. It can be seen that for CaF our results are on the average distinctly closer to experiment than all previous calculations. For BaF our results also compare well with the previous theoretical work. The polarization model performs best in this case, although it should be remembered that this theory contains a freely adjustable parameter.

D. Wave functions and low-energy behavior of the quantum defects

Ernst and Kändler[38] have measured the electric dipole moments of some of the lower states of CaF. They found vastly different values for the $A\ ^2\Pi$ and $C\ ^2\Pi$ states and interpreted this in terms of two distinct types of polarization of the lone electron orbital. In the first case the electron is polarized away from the X^- center ($X\ ^2\Sigma^+$ or $A\ ^2\Pi$ state)

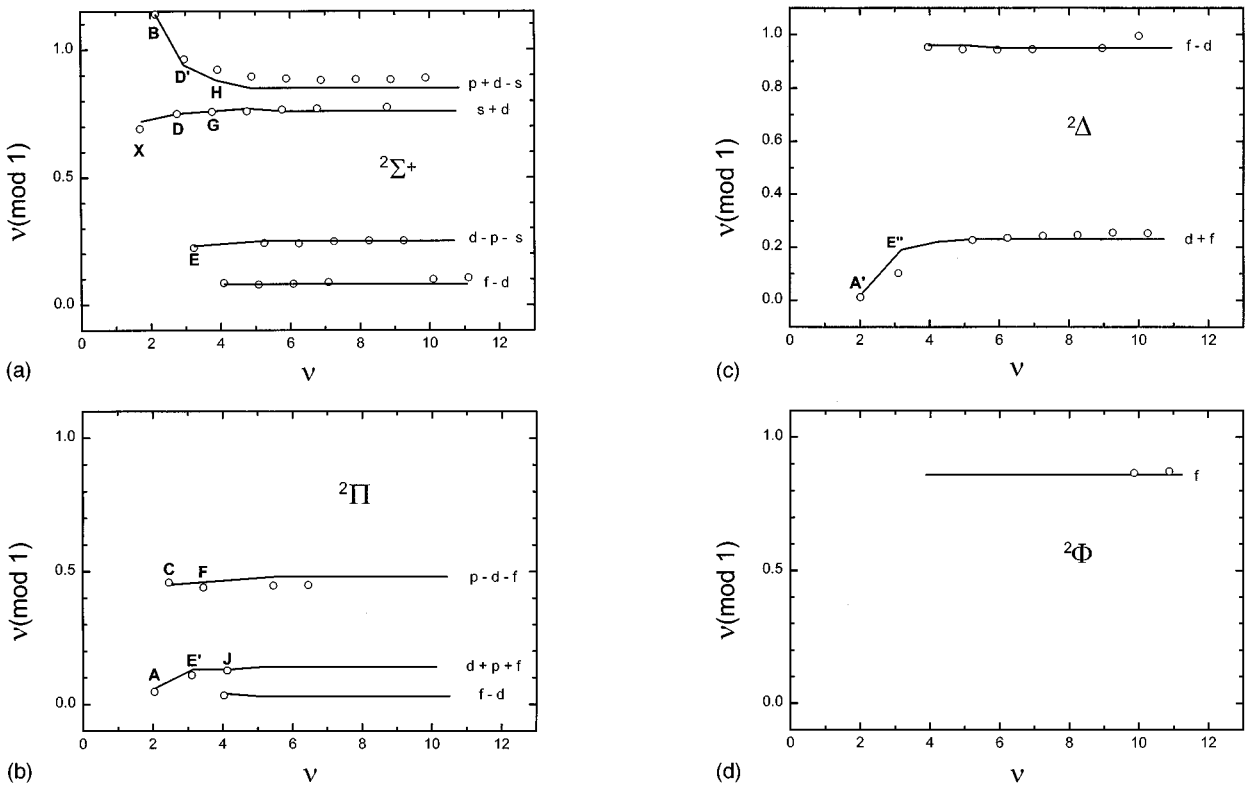

FIG. 5. Rydberg series of BaF, Cf. caption for Fig. 4.

and the core dipole moment is partly compensated. In the second case so-called ''reversed'' polarization of the Rydberg electron occurs towards the X^- center and the total dipole moment, core plus Rydberg electron, is on the contrary increased. This behavior has been confirmed by the *ab initio* calculations of Bündgen *et al.*[3] for the two states. Murphy *et al.*[7] further related this to the low-ν behavior of ν(mod1); low states undergoing ''normal'' polarization are stabilized in the attractive potential well of M^{++}, whereas low states undergoing ''reversed'' polarization are destabilized. In the plots of Figs. 4 and 5 this becomes manifest in the characteristic positive slope/negative curvature or negative slope/positive curvature of the ν(mod1) vs ν curves in the two cases, although this behavior is not equally pronounced in all the series. These conjectures are again confirmed qualitatively by the present calculations and shown to

TABLE V. The lowest electronic states of CaF: Various theoretical results (cm^{-1}).

		Present[a]		*Ab initio*[b]		Pol. model[c]		Ligand field[d]	
	Obs, T_0	Calc	*o-c*	Calc	*o-c*	Calc	*o-c*	Calc	*o-c*
$X\ ^2\Sigma^+$	0	1 407	−1 407	0	0	0	0	0	0
$A\ ^2\Pi$	16 530[e]	16 883	−353	17 712	−1 182	16 340	+190	18 217	−1 687
$B\ ^2\Sigma^+$	18 841[f]	20 148	−1 307	20 069	−1 228	18 620	+221	21 486	−2 645
$B'\ ^2\Delta$	21 544[g]	23 259	−1 715	24 851	−3 307	17 690	+3 854	22 552	−1 008
$D\ ^2\Sigma^+$	30 159[h]	30 253	−94	32 741	−2 582	…	…	…	…
$C\ ^2\Pi$	30 216[h]	30 122	+94	32 765	−2 549	29 850	+366	32 138	−1 922
Mean deviation			1 062		2 121		1 738		1 709

[a]This work. T_0 values, obtained by correcting the calculated vertical ionization energies for the differences of vibrational frequency and internuclear distance in the molecular state and the ion.
[b]P. Bündgen, B. Engels, and S. D. Peyerimhoff, Ref. 3.
[c]T. Törring, W. E. Ernst, and J. Kändler, Ref. 2.
[d]A. R. Allouche, G. Wannous, and M. Aubert-Frécon, Ref. 37.
[e]P. F. Bernath and R. W. Field, Ref. 30.
[f]M. Dulick, P. F. Bernath, and R. W. Field, Ref. 27.
[g]J. Vergès, C. Effantin, A. Bernard, A. Topouzkhanian, A. R. Allouche, J. D'Incan, and R. F. Barrow, Ref. 5.
[h]C. M. Gittins, N. A. Harris, R. W. Field, J. Vergès, C. Effantin, A. Bernard, J. D'Incan, W. E. Ernst, P. Bündgen, and B. Engels, Ref. 29.

TABLE VI. The lowest electronic states of BaF: Various theoretical results (cm^{-1}).

		Present[a]		*Ab initio*[b]		Pol. model[c]		Ligand field[d]	
	Obs, T_0	Calc	*o-c*	Calc	*o-c*	Calc	*o-c*	Calc	*o-c*
$X\ ^2\Sigma^+$	0	1 245	−1 245	0	0	0	0	0	0
$A'\ ^2\Delta$	10 939[e]	11 150	−211	7 420	+3 519	11 100	−161	11 310	−371
$A\ ^2\Pi$	11 980[e]	12 309	−329	9 440	+2 540	12 330	−350	11 678	+302
$B\ ^2\Sigma^+$	13 945[e]	13 962	−17	12 660	+1 285	14 250	−305	13 381	+564
$C\ ^2\Pi$	20 086[f]	19 956	+130	16 290	+3 796	19 970	+116	22 080	−1 994
$D\ ^2\Sigma^+$	24 177[f]	24 231	−54	25 810	−1 633	⋯	⋯	⋯	⋯
$D'\ ^2\Sigma^+$	26 245[g]	26 046	+199	32 750	−6 505	⋯	⋯	⋯	⋯
Mean deviation			502		3 378		226		951

[a]This work. T_0 values, obtained by correcting the calculated vertical ionization energies for the differences of vibrational frequency and internuclear distance in the molecular state and the ion.
[b]E. Westin and A. Rosen, Ref. 4.
[c]T. Törring, W. E. Ernst, and J. Kändler, Ref. 2.
[d]A. R. Allouche, G. Wannous, and M. Aubert-Frécon, Ref. 37.
[e]A. Bernard, C. Effantin, J. D'Incan, J. Vergès, and R. F. Barrow, Ref. 35.
[f]C. Effantin, A. Bernard, J. D'Incan, G. Wannous, J. Vergès, and R. F. Barrow, Ref. 32.
[g]A. Bernard, C. Effantin, E. Andrianavalona, J. Vergès, and R. F. Barrow, Ref. 6.

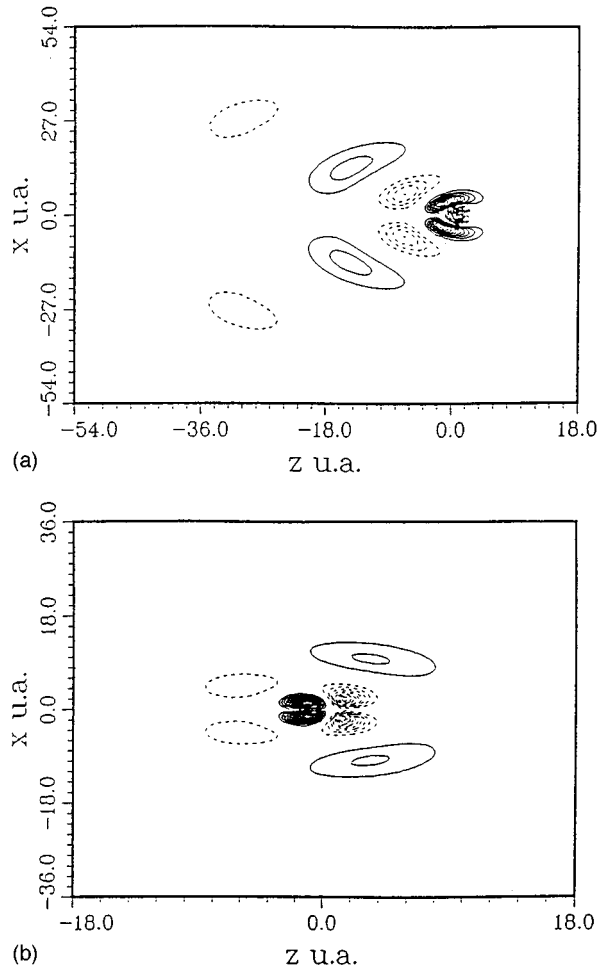

FIG. 6. Wave function contour plots for BaF $^2\Pi$ series near $\nu\approx5$. $z=0$ corresponds to the position of the Ba nucleus. The F nucleus is situated at $z=4$. Full and dotted lines are used to indicate sign changes of the wave function. (a) 0.13Π series. (b) 0.45Π series.

hold for the whole series as demonstrated for the BaF 0.13Π (terminus state $A\ ^2\Pi$) and 0.45Π (terminus state $C\ ^2\Pi$) series near $\nu\approx5$. The electron wave function contour plot of Fig. 6(a) shows strong polarization away from X^- in the former case, whereas Fig. 6(b) on the contrary shows appreciable probability amplitude in the vicinity of X^- in the latter case.

E. States with high orbital angular momentum

Tables VII(a) and VII(b) list for CaF and BaF, respectively, the effective principal quantum numbers calculated for the lowest nonpenetrating states with $\tilde{l}=4-6$. As indicated earlier we set all quantum defects $\mu_{\tilde{l}',\tilde{l}}$ for $\tilde{l}',\tilde{l}\geq4$ identically to zero in these calculations. The resulting effective quantum defects μ are thus due entirely to the departure of the potential given by Eqs. (12) and (13) from that of a single point charge Z_1+Z_2.

Watson[39] recently derived a formula for calculating the quantum defect of an electron moving in the field of an elec-

TABLE VII. (a) Nonpenetrating Rydberg states of CaF.[a] (b) Nonpenetrating Rydberg states of BaF.

λ=	0	1	2	3	4	5	6
				(a)			
$\tilde{l}=4$	5.038	5.031	5.011	4.981	4.943		
5	6.021	6.018	6.012	6.001	5.986	5.968	
6	7.013	7.012	7.009	7.004	6.998	6.990	6.980
				(b)			
$\tilde{l}=4$	5.036	5.029	5.009	4.978	4.941		
5	6.020	6.018	6.011	6.000	5.985	5.966	
6	7.012	7.011	7.008	7.004	6.997	6.989	6.979

[a]Each entry corresponds to the calculated effective quantum number of the lowest state for the $\tilde{l}$ and λ values indicated.

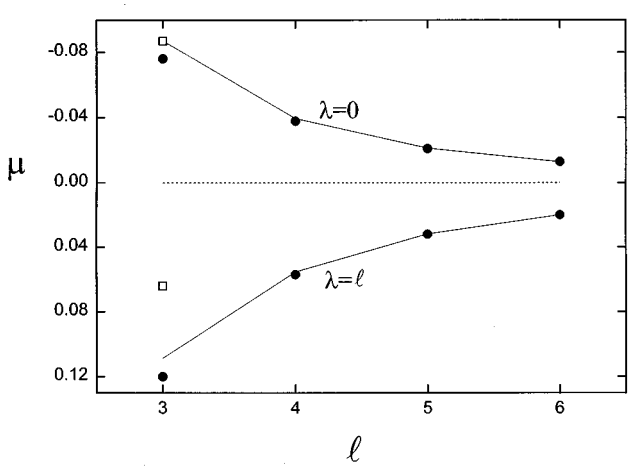

FIG. 7. Quantum defects of high-$\tilde{l}$ states of CaF for $\lambda=0$ (highest-energy component) and $\lambda=\tilde{l}$ (lowest-energy component). Note that, in line with Figs. 4 and 5, $-\mu$ has been plotted. Full lines, point dipole model [Eqs. (27) and (28)]. Circles, numerical values [Eq. (20)]. Squares, experimental values.

tric point charge with a superposed point dipole. It is instructive to compare the quantum defects derived from the effective principal quantum numbers ν of Tables VII(a) and VII(b) with those obtained from Watson's analytical expression. For unit total charge his formula gives

$$\mu_{l,\lambda}=-\frac{2[l(l+1)-3\lambda^2]}{(2l+3)(2l+1)(2l-1)l(l+1)}\,(Q_1^2-Q_2), \tag{27}$$

where Q_1 is the dipole and Q_2 the quadrupole moment. Watson showed that while both these quantities are origin-dependent for a system carrying a net electronic charge, the combination $Q_1^2-Q_2/(Z_1+Z_2)$ is origin-independent as physically required. Here we take the midpoint between the two nuclei as the center and we find from Eqs. (12) and (24) that

$$Q_1^2-Q_2=\frac{R^2}{4}\,[(Z_2^{\rm eff}-Z_1^{\rm eff})^2-1] \tag{28}$$

with $Z_1^{\rm eff}$ and $Z_2^{\rm eff}$ defined by Eq. (13). Figure 7 compares the quantum defects obtained from Eqs. (27) and (28) by using the appropriate α_1, α_2, and R values for CaF from Table II, with l taken equal to $\tilde{l}$ and with the quantum defect values derived from Table VII(a). It can be seen that the two sets of values are indeed in close agreement. Notice that the values calculated with the present numerical elliptical approach appear consistently somewhat lower in the plot of Fig. 7 than those derived from Watson's model. This is due to the ξ-dependent polarization term included in Eq. (12) which adds a contribution

$$\Delta\mu_l^{\rm Pol}(\epsilon)=(\alpha_1+\alpha_2)\,\frac{3-l(l+1)\epsilon}{4\left(l-\frac{1}{2}\right)l\left(l+\frac{1}{2}\right)(l+1)\left(l+\frac{3}{2}\right)} \tag{29}$$

to the quantum defect. (There are further small polarization terms which we neglect here.) Equation (29) yields contributions 0.010, 0.003, and 0.001 to the quantum defects for $l=4-6$, respectively, which correspond closely to the deviations apparent in Fig. 7. We conclude that for the bound state range considered in this work nonpenetrating states with $\tilde{l}\geqslant 4$, and in fact very nearly also the states derived from $\tilde{l}=3$ orbitals, can be calculated directly from Eqs. (27)–(29) without use of the numerical apparatus developed in the earlier sections of this paper.

V. CONCLUSION

In this work we have developed a theoretical approach designed to calculate the electronic structure of ionic diatomic ions with an associated electron, based solely on the properties of the constituent ions such as their charges and dipole polarizabilities. For the lowest bound states our approach resembles in many ways the ligand-field model of Rice, Martin, and Field[1] and the electrostatic polarization model of Törring, Ernst, and Kändler.[2] It yields however an equally good description for the high Rydberg states and has led, in the application to the CaF and BaF molecules, to the first quantitative calculation of the full electronic spectrum of these molecules at equilibrium.

Obvious further applications of this approach will be to some of the other alkaline earth halides whose Rydberg spectrum is not yet known in detail and where we should be able to make reliable predictions. The rare gas hydrides constitute another class of ionic systems where one has $Z_1=0$ and $Z_2=+1$ instead of $Z_1=+2$ and $Z_2=-1$, i.e., the ion core may be represented as a protonated rare gas atom. We will show in a forthcoming paper that with this simple substitution the present theory accounts equally well for the electronic structure of ArH and KrH as for the alkaline earth halides studied here. Further, the present method is by no means restricted to Rydberg molecules with $Z_1+Z_2=+1$. It might also be applied to the calculation of electron phase shifts in negative ions possessing a double-closed-shell neutral core ($Z_1+Z_2=0$) such as, e.g., alkali-halides. An interesting future avenue which we hope to pursue is the extension of the method to treat Rydberg states of small van der Waals complexes, a subject that is just beginning to emerge experimentally. Polyatomic systems with a protonated closed-shell core constitute another class of possible candidates for the method; HCO is an example whose Rydberg spectrum is under study by Grant and co-workers.[40]

There are two obvious limitations of the approach such as it has been outlined here. First, by representing the ligand ion as a point charge we have neglected electron penetration effects on the second center beyond those taken into account by the polarization potential used here. The results seem to indicate that this approximation is reasonable. R matrix calculations allowing for two excluded atomic zones, one around each atomic nucleus, clearly constitute the required next step in the development of the method. The conceptual link with the multiple scattering (MSM) model of Dill and Dehmer[11] will then become clearly apparent. However our

approach, once extended, will not be restricted to the case of a constant potential between the scattering centers and should thus yield a more realistic description of electron-molecule multiple scattering. A more serious drawback of the approach is that in the molecular reaction zone II a one-electron Hamiltonian is employed. Thus the mixing of the $M^{++}X^{-}e^{-}$ configurations with configurations of the type $M^{+}Xe^{-}$ occurring in the alkaline earth halides as dissociation is approached, is beyond the present framework.

Small-amplitude vibrations around the equilibrium on the other hand can be handled without difficulty at present. In a forthcoming paper[10] we shall evaluate the derivatives with respect to R of the quantum defect matrices, i.e., those quantities that yield the contribution of the Rydberg electron to the bond strength as well as the vibronic coupling that affects the manifold of high Rydberg states.[41] Calculations of spin–orbit splittings and permanent and transition dipole moments will also be presented.

Returning once again to the CaF and BaF molecules, we stress that our calculations unambiguously establish the low-energy terminus states for all of the Rydberg series. In particular, the four $\tilde{f}$ series are nearly nonpenetrating in both molecules, and have in fact almost the same quantum defects in CaF and BaF due entirely to the core dipole plus quadrupole field of the molecular ion core. Their lowest members have $\nu \approx 4$ for all λ components. This is somewhat unexpected since the atomic f orbital is nonpenetrating in Ca^{+} but penetrating in Ba^{+}. We shall show in Ref. 10 that the molecular $\tilde{f}$ orbitals of BaF indeed become more and more penetrating as the energy increases beyond the range studied so far. The formula of Watson[39] then fails for their description, and use of the full R-matrix apparatus becomes again necessary.

ACKNOWLEDGMENTS

We thank M. Aymar (Orsay) for providing the computer code for solving the generalized eigenvalue problem. Many enlightening discussions with her and with R. W. Field (MIT) are gratefully acknowledged. N. Shafizadeh (Orsay) helped with the design of the figures. W. E. Ernst (Pennsylvania State University) and E. Luc-Koenig (Orsay) are thanked for their remarks regarding the manuscript.

APPENDIX A: BOX QUANTIZATION WITH ARBITRARY BOUNDARY CONDITIONS

We wish to determine the eigenenergies and eigenfunctions of the one-dimensional free-particle radial Hamiltonian in a box $r_a \leqslant r \leqslant r_b$ in such a way that

$$-\frac{\psi'}{\psi}=b_a, \quad r=r_a, \quad -\frac{\psi'}{\psi}=b_b, \quad r=r_b, \tag{A1}$$

where b_a and b_b are given. The general expression of the wave function for positive energy, $\epsilon=k^2 \geqslant 0$ is given by

$$\psi=\frac{1}{N}\left[c\ \sin(kr)+d\ \cos(kr)\right], \tag{A2}$$

where N normalizes ψ to unity. It is easy to show that the quantization condition is given by

$$(b_a b_b+k^2)\sin(kr_a-kr_b)-k(b_a-b_b)\cos(kr_a-kr_b)=0, \tag{A3}$$

while the ratio of the coefficients c and d is

$$\frac{c}{d}=-\frac{b_a\ \cos(kr_a)-k\ \sin(kr_a)}{b_a\ \sin(kr_a)+k\ \cos(kr_a)}. \tag{A4}$$

The normalization factor N is obtained as

$$N^2=\frac{1}{2}\ (c^2+d^2)(r_a-r_b)-\frac{1}{4k}\ (c^2-d^2)[\sin(2kr_b) - \sin(2kr_a)]+\frac{cd}{k}\ [\sin^2(kr_b)-\sin^2(kr_a)]. \tag{A5}$$

For certain boundary conditions b_a and b_b one may also have a solution at negative energy, $\epsilon=-\kappa^2 \leqslant 0$. In this case Eq. (A2) becomes

$$\psi=\frac{1}{N}\left[ce^{+\kappa r}+de^{-\kappa r}\right], \tag{A6}$$

whereas the quantization condition becomes

$$(b_a b_b-\kappa^2)\sinh(\kappa r_a-\kappa r_b)-\kappa(b_a-b_b) \times \cosh(\kappa r_a-\kappa r_b)=0. \tag{A7}$$

The analog of Eq. (A4) is now

$$\frac{c}{d}=-\frac{(b_a-\kappa)e^{-\kappa r_a}}{(b_a+\kappa)e^{+\kappa r_a}}, \tag{A8}$$

while the normalization factor is

$$N^2=\frac{c^2}{2\kappa}\ (e^{2\kappa r_b}-e^{2\kappa r_a})-\frac{d^2}{2\kappa}\ (e^{-2\kappa r_b}-e^{-2\kappa r_a}) +2cd(r_b-r_a). \tag{A9}$$

We have found that in order to attain convergence in the R-matrix calculations it is important to include states at negative energy, Eq. (A6), in addition to states at positive energy, Eq. (A2).

APPENDIX B: THE TWO-CENTER PROBLEM IN ELLIPTICAL COORDINATES

The kinetic energy operator expressed in the elliptical coordinates of Eq. (11) is[42]

$$\Delta=\frac{4}{R^2(\xi^2-\eta^2)}\left[\frac{\partial}{\partial\xi}\ (\xi^2-1)\ \frac{\partial}{\partial\xi}+\frac{1}{\xi^2-1}\ \frac{\partial^2}{\partial\phi^2} + \frac{\partial}{\partial\eta}\ (1-\eta^2)\ \frac{\partial}{\partial\eta}+\frac{1}{1-\eta^2}\ \frac{\partial^2}{\partial\phi^2}\right]. \tag{B1}$$

The Schrödinger equation for a single electron in Rydberg energy units is then

$$[\Delta-V+\epsilon]\Psi=0, \tag{B2}$$

where the potential energy V is given by Eq. (12). Writing

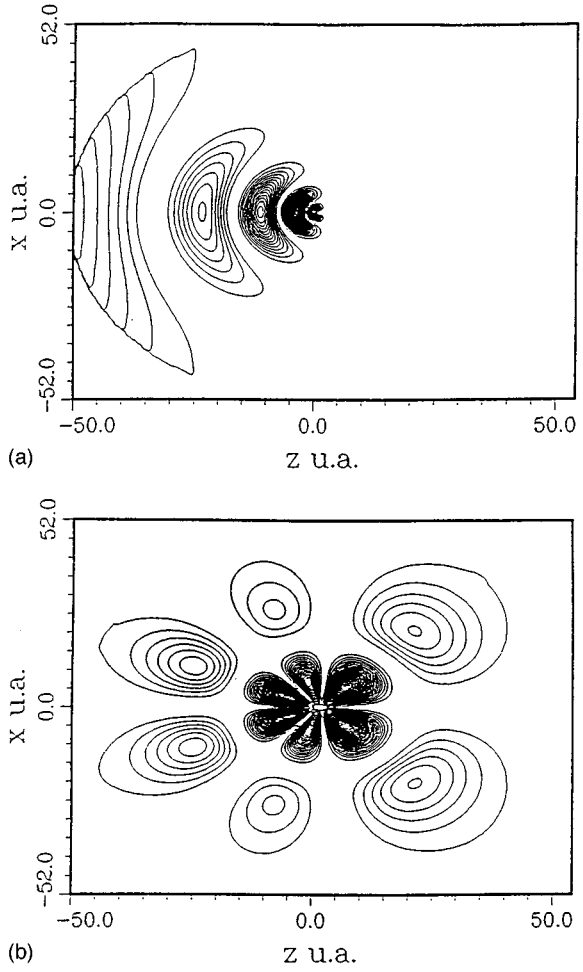

FIG. 8. Contour plots of elliptic orbitals evaluated for BaF with the parameters from Table II and Eqs. (12) and (13). $z=0$ corresponds to the position of the Ba nucleus. The F nucleus is situated at $z=4$. Note that the wave functions have been evaluated only for $\xi<27$. (a) $5\tilde{s}\sigma$. (b) $5\tilde{f}\pi$.

$$\Psi(\xi,\eta,\phi)=\frac{1}{\sqrt{\xi^2-1}}\,\tilde{X}(\xi)\tilde{Y}(\eta,\phi), \tag{B3}$$

and replacing $\partial^2/\partial\phi^2$ by $-\lambda^2$ we obtain separate angular and radial equations,

$$\left[\frac{\partial}{\partial\eta}(1-\eta^2)\,\frac{\partial}{\partial\eta}-\frac{\lambda^2}{(1-\eta^2)}-(Z_1^{\rm eff}-Z_2^{\rm eff})R\eta+p^2\eta^2 -A(\epsilon)\right]\tilde{Y}(\eta,\phi)=0, \tag{B4}$$

where $p^2=-\epsilon R^2/4$ and the ϕ dependent factor contained in $\tilde{Y}$ is simply $(2\pi)^{-1/2}e^{i\lambda\phi}$, and

$$\left\{\frac{\partial}{\partial\xi}(\xi^2-1)\,\frac{\partial}{\partial\xi}-\frac{\lambda^2}{(\xi^2-1)}+\left[(Z_1+Z_2)+\frac{4}{R^3\xi^3} \times(\alpha_1+\alpha_2)f\right]R\xi-p^2\xi^2+A(\epsilon)\right\}\frac{1}{\sqrt{\xi^2-1}}\,\tilde{X}(\xi)=0, \tag{B5}$$

where $A(\epsilon)$ is the separation constant and f is a cutoff function analogous to Eq. (3). Setting

$$\tilde{Y}(\eta,\phi)=\frac{1}{\sqrt{1-\eta^2}}\,Y(\eta,\phi) \tag{B6}$$

in order to have only second derivatives we obtain

$$\left\{\frac{\partial^2}{\partial\eta^2}-\frac{1}{1-\eta^2}\left[\frac{\lambda^2-1}{1-\eta^2}+(Z_1^{\rm eff}-Z_2^{\rm eff})R\eta-p^2\eta^2\right] +\frac{1}{1-\eta^2}\left[-A(\epsilon)\right]\right\}\times Y(\eta,\phi)=0, \tag{B7}$$

$$\left(\frac{\partial^2}{\partial\xi^2}-\frac{1}{\xi^2-1}\left\{\frac{\lambda^2-1}{\xi^2-1}-\left[(Z_1+Z_2)+\frac{4}{R^3\xi^3}\,(\alpha_1 +\alpha_2)f\right]R\xi-A(\epsilon)\right\}+\left[\frac{R^2\xi^2}{4(\xi^2-1)}\right]\epsilon\right)\tilde{X}(\xi)=0. \tag{B8}$$

The angular function $\tilde{Y}$ in Eqs. (B3) and (B6) is the same as that occurring in Eq. (14). We obtain the discrete eigenvalue spectrum of A by numerical integration of Eq. (B7) with the appropriate bound state boundary conditions applied at $\eta=-1$ and $\eta=+1$. The eigenfunctions Y of Eq. (B7) behave as $(1\pm\eta)^{(1+\lambda)/2}$ near $\eta=\mp1$, respectively. The eigenvalues A reduce for $p=0$ to the familiar quantity $l(l+1)$. In analogy with the spherical problem we define the generalized orbital angular momentum quantum number as

$$\tilde{l}=k_\eta+\lambda, \tag{B9}$$

where k_η is the number of nodes of the eigenfunction of Eq. (B7). Multiplication of the eigenfunction of Eq. (B7) by $(2\pi)^{-1/2}e^{i\lambda\phi}$ yields $\tilde{Y}(\eta,\phi)$. $\tilde{Y}$ is normalized to unity with a volume element $d\eta d\phi$.

Once $\tilde{Y}$ and A have been obtained for the given energy ϵ and values $\tilde{l}$ and λ, Eq. (B8) is integrated and, depending on the boundary conditions imposed for $\xi=1$ and $\xi=\infty$ following the methods of Refs. 16 and 15, the energy-normalized regular solution $\tilde{X}=\tilde{f}$ or the irregular solution $\tilde{X}=\tilde{g}$ will be obtained. For $\lambda>0$ $\tilde{f}$ behaves as $(\pi\lambda)^{-1/2}(\xi-1)^{(1+\lambda)/2}$ near $\xi\approx1$, whereas $\tilde{g}$ behaves as $-(\pi\lambda)^{-1/2}(\xi-1)^{(1-\lambda)/2}$. For $\lambda=0$ $\tilde{f}$ behaves as $(\xi-1)^{1/2}$ near $\xi\approx1$, whereas $\tilde{g}$ behaves as $(\pi)^{-1}(\xi-1)^{1/2}\ln(\xi-1)$. Equation (14) is a superposition of functions of the type of Eq. (B3). The volume element for the total wave function is $R^3(\xi^2-\eta^2)d\xi d\eta d\phi/8$.

Figure 8 shows two examples of contour plots of elliptical BaF orbitals $\tilde{Y}_{\tilde{l}\lambda}(\eta,\phi=0)\tilde{f}_{\tilde{l}}(\xi)$. Strong polarization away from the halogen ion is apparent for low $\tilde{l}$ and λ, whereas for higher $\tilde{l}$ and λ the familiar shapes of hydrogenic orbitals are recovered.

[1] S. F. Rice, H. Martin, and R. W. Field, J. Chem. Phys. **82**, 5023 (1985).
[2] T. Törring, W. E. Ernst, and J. Kändler, J. Chem. Phys. **90**, 4927 (1989).
[3] P. Bündgen, B. Engels, and S. D. Peyermhoff, Chem. Phys. Lett. **176**, 407 (1991).
[4] E. Westin and A. Rosen, Chem. Phys. Lett. **149**, 239 (1988).
[5] J. Vergès, C. Effantin, A. Bernard, A. Topouzkhanian, A. R. Allouche, J. D'Incan, and R. F. Barrow, J. Phys. B **26**, 279 (1993).
[6] A. Bernard, C. Effantin, E. Andrianavalona, J. Vergès, and R. F. Barrow, J. Mol. Spectrosc. **152**, 174 (1992).

[7] J. E. Murphy, J. M. Berg, A. J. Merer, N. A. Harris, and R. W. Field, Phys. Rev. Lett. **65**, 1861 (1990).
[8] Z. J. Jakubek and R. W. Field, Phys. Rev. Lett. **72**, 2167 (1994).
[9] N. A. Harris and Ch. Jungen, Phys. Rev. Lett. **70**, 2549 (1993).
[10] M. Arif, Ch. Jungen, and A. L. Roche (in preparation).
[11] Dan Dill and J. L. Dehmer, J. Chem. Phys. **61**, 692 (1974).
[12] M. Philippe, F. Masnou-Seeuws, and P. Valiron, J. Phys. B **12**, 2493 (1979).
[13] N. Y. Du and C. H. Greene, Phys. Rev. A **36**, 971 (1987).
[14] M. J. Seaton, Rep. Prog. Phys. **46**, 167 (1983).
[15] F. Texier and Ch. Jungen (in preparation).
[16] C. H. Greene, A. R. P. Rau, and U. Fano, Phys. Rev. A **26**, 2441 (1982).
[17] U. Fano and C. M. Lee, Phys. Rev. Lett. **31**, 1573 (1973).
[18] C. H. Greene, Phys. Rev. A **28**, 2209 (1983).
[19] G. Miecznik and C. H. Greene, Chem. Phys. Lett. **258**, 607 (1996).
[20] M. Aymar and M. Telmini, J. Phys. B **24**, 4935 (1991).
[21] T. Törring, W. E. Ernst, and S. Kindt, J. Chem. Phys. **81**, 4614 (1984).
[22] Z. J. Jakubek, N. A. Harris, R. W. Field, J. A. Gardner, and E. Murad, J. Chem. Phys. **100**, 622 (1994).
[23] G. H. F. Diercksen and A. J. Sadlej, Mol. Phys. **47**, 33 (1982).
[24] Z. Jakubek (private communication, 1994).
[25] C. H. Greene and M. Aymar, Phys. Rev. A **44**, 1773 (1991).
[26] J. M. Berg, J. E. Murphy, N. A. Harris, and R. W. Field, Phys. Rev. A **48**, 3012 (1993).
[27] M. Dulick, P. F. Bernath, and R. W. Field, Can. J. Phys. **58**, 703 (1980).
[28] N. A. Harris and R. W. Field, J. Chem. Phys. **98**, 2642 (1993).
[29] W. E. Ernst, J. Kändler, and O. Knüppel, J. Mol. Spectrosc. **153**, 81 (1992); see also, C. M. Gittins, N. A. Harris, R. W. Field, J. Vergès, C. Effantin, A. Bernard, J. d'Incan, W. E. Ernst, P. Bündgen, and B. Engels, *ibid*. **161**, 303 (1993).
[30] P. F. Bernath and R. W. Field, J. Mol. Spectrosc. **82**, 339 (1980).
[31] R. W. Field, N. A. Harris, and Ch. Jungen (in preparation).
[32] C. Effantin, A. Bernard, J. D'Incan, G. Wannous, J. Vergès, and R. F. Barrow, Mol. Phys. **70**, 735 (1990).
[33] Z. J. Jakubek and R. W. Field, J. Mol. Spectrosc. **179**, 99 (1996).
[34] Z. J. Jakubek, Thesis, Massachusetts Institute of Technology, 1995.
[35] A. Bernard, C. Effantin, J. D'Incan, J. Vergès, and R. F. Barrow, Mol. Phys. **70**, 747 (1990).
[36] C. Effantin, A. Bernard, J. D'Incan, E. Adrianavalona, and R. F. Barrow, J. Mol. Spectrosc. **145**, 456 (1991).
[37] A. R. Allouche, G. Wannous, and M. Aubert-Frécon, Chem. Phys. **170**, 11 (1993).
[38] W. E. Ernst and J. Kändler, Phys. Rev. A **39**, 1575 (1989).
[39] J. K. G. Watson, Mol. Phys. **81**, 277 (1994); cf. also B. A. Zon, Sov. Phys. JETP **75**, 19 (1992).
[40] E. Mayer and E. R. Grant, J. Chem. Phys. **103**, 5361 (1995).
[41] See, e.g., C. H. Greene and Ch. Jungen, Adv. At. Mol. Phys. **21**, 51 (1985).
[42] D. R. Bates, K. Ledsham, and A. L. Stewart, Proc. R. Soc. London **246**, 28 (1953).